ESD-TR-67-282

ESD-TR-67-282
ESTI FILE COPY

THIRD QUARTERLY TECHNICAL REPORT ON
LARGE APERTURE SEISMIC ARRAYS

March 1967

DIRECTORATE OF PLANNING AND TECHNOLOGY
ELECTRONIC SYSTEMS DIVISION
AIR FORCE SYSTEMS COMMAND
UNITED STATES AIR FORCE
L. G. Hanscom Field, Bedford, Massachusetts

Sponsored by:

Advanced Research Projects Agency, Washington, D. C.
ARPA Order No. 800

Distribution of this document
is unlimited.

ESL-2

AD0651653

LEGAL NOTICE

OTHER NOTICES

ESD-TR-67-282

THIRD QUARTERLY TECHNICAL REPORT ON
LARGE APERTURE SEISMIC ARRAYS

March 1967

DIRECTORATE OF PLANNING AND TECHNOLOGY
ELECTRONIC SYSTEMS DIVISION
AIR FORCE SYSTEMS COMMAND
UNITED STATES AIR FORCE
L. G. Hanscom Field, Bedford, Massachusetts

FOREWORD

This research was supported by the Advanced Research
Projects Agency. The Electronic Systems Division technical
project officer for Contract AF 19(628)-5981 is Major Cleve
P. Malone (ESL-2)

This technical report has been reviewed and is approved.

PAUL W. RIDENOUR, Lt. Col., USAF
Chief, LASA Office
Directorate of Planning and Technology
Electronic Systems Division

ABSTRACT

A progress report on three topics that were studied
during the third quarter of Contract AF19(628)-5981 is pre-
sented. Preliminary results on spectral estimates of seis-
mic events are presented and two principal conclusions are
suggested: noise prediction is probably not a useful means
of reducing the variability of spectral estimates, and, for
the one large surface-focus event processed to date, there
is a significant amount of signal energy above 4 Hz. The
problem of detecting nuclear explosions in the presence of
large natural events has also been considered during this
period. This problem is discussed here, with the emphasis on
the possibility of "steering" nulls at the natural events.
Difficulties resulting from the sampled nature of the seismic
records and from coda reverberations are also discussed in
this context. Finally, the location of epicenters by beam-
splitting with a LASA is discussed. The technique is de-
scribed, the sources of error are analyzed, and data from
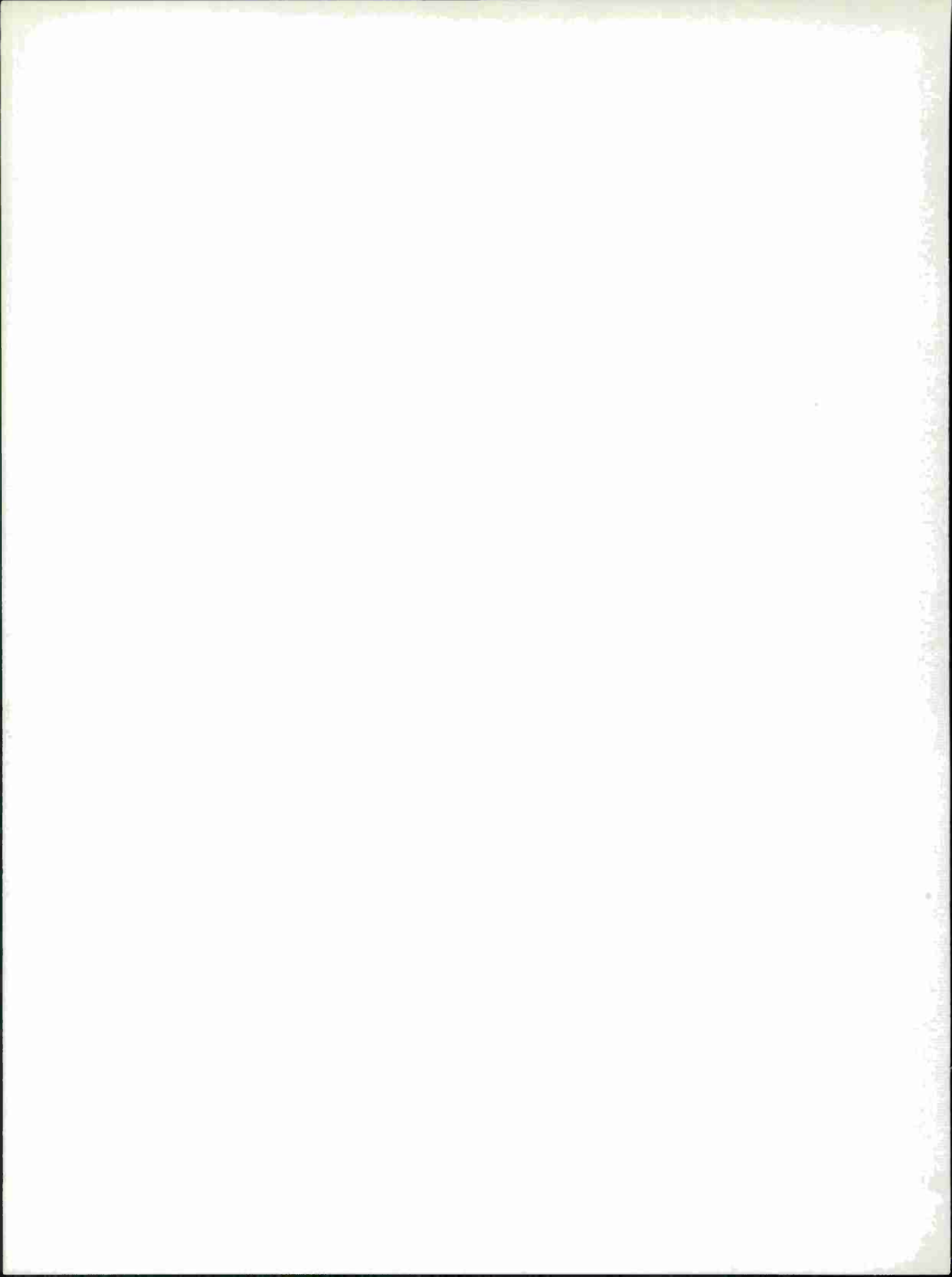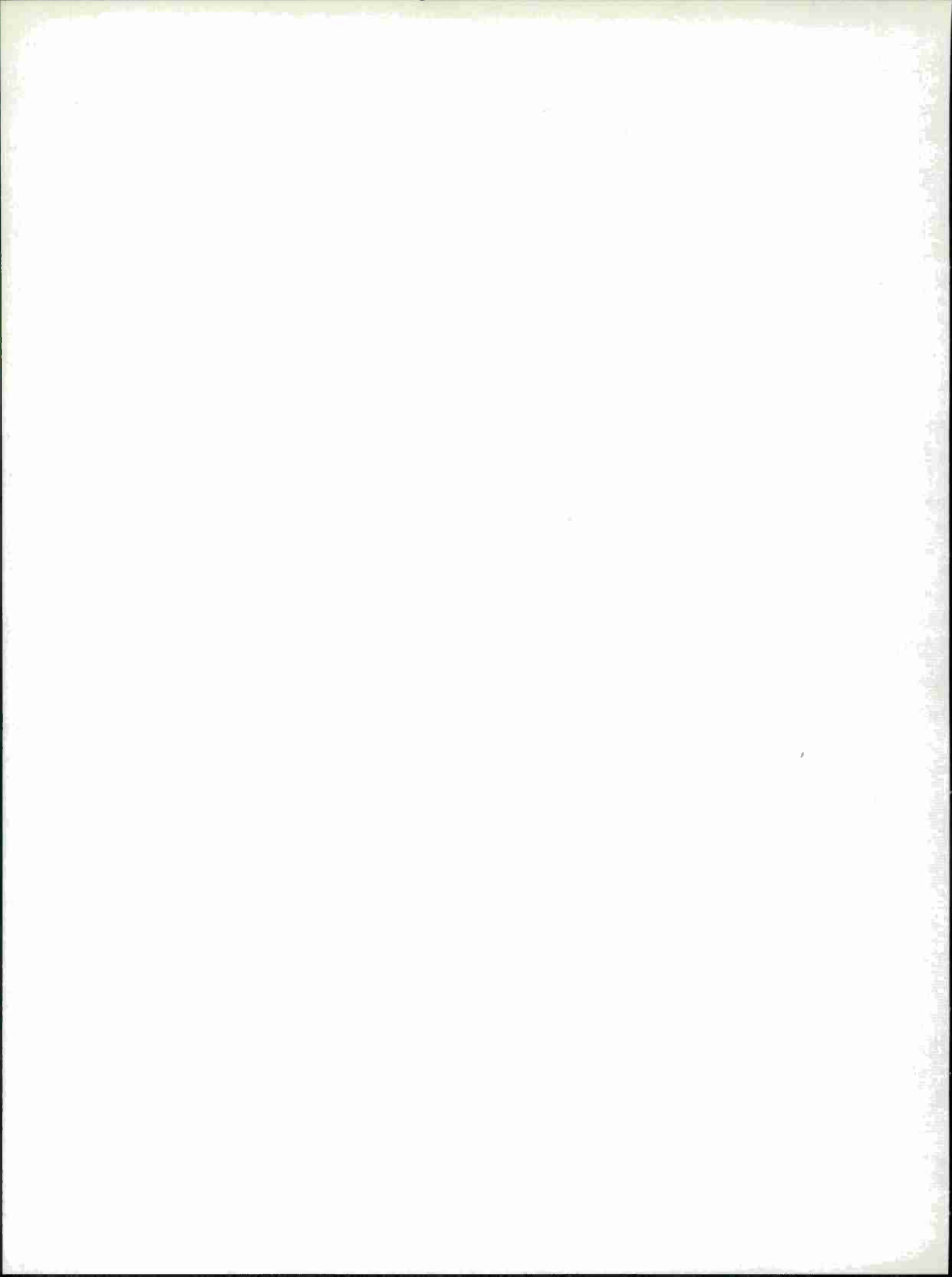three seismic events are presented.

TABLE OF CONTENTS

LIST OF FIGURES

LIST OF FIGURES

SECTION I

INTRODUCTION

This is the third quarterly report on Contract AF19(628)-5981. It covers the period from September 15 to December 15, 1966. Three topics are discussed in this report. Section II consists of presentation of preliminary results using the spectral estimation techniques discussed in the last quarterly report. The suppression of signals from large earthquakes for the purpose of detecting lower magnitude events that are close in both time and space to the large event is discussed in Section III. The coherent use of the elements of LASA to locate the epicenter of events with this array alone is considered in Section IV, and the results of some preliminary calculations are presented. As these three topics are rather disjoint, introductory and concluding remarks concerning each topic appear separately in the appropriate sections.

All three discussions are status reports only, for much more work remains to be done on each of the topics discussed. In the case of spectral estimation, only one event has been studied to date. This one event, however, shows substantial signal-to-noise ratio out to at least 4 Hz. The study of large event suppression has reached the point of discarding array nulls as impractical, and is now progressing to a study of continental sized arrays. Finally, first efforts at "beam-splitting" for precise epicenter determination from LASA are in their infancy but certain methods of refining these calculations are clearly indicated and will be pursued in the immediate future.

SECTION II

SPECTRAL ESTIMATES OF SEISMIC EVENTS

This chapter consists of a progress report on work
relating to the estimation of the energy density spectra of
seismic events. The theoretical basis for this work was pre-
sented in Section III of the last report[1]. Following the
preparation of that report, the computer programs necessary
to implement the desired calculations were developed. To
date these calculations have been applied to one seismic
record which included a large surface-focus event and to
three additional records (from the same seismometer) consist-
ing only of noise. Some of the results of these calculations
are presented in this chapter.

It should be stressed that these are very preliminary
results, the calculations being based on a single seismic
event and only a few noise records. However, these calcula-
tions are sufficient to tentatively conclude that noise pre-
diction will not be a useful tool in spectral estimation of
seismic events and to give some sample results on seismic
spectra.

This chapter begins with a brief review of the theoreti-
cal discussion of the previous report. In this review the
equations are restated in the finite-discrete formulation ap-
propriate for the digital computer implementation. This is
followed by a brief discussion of some of the programming con-
siderations involved in carrying out these calculations. The
next section presents the experimental results of the noise
prediction calculation. This is followed by a discussion of
the results of the spectral calculations. These calculations
involve two choices of time windows and were performed on
seismic records before and after high-pass filtering. The
final section consists of tentative conclusions and recommen-
dations for continued work on this project.

2.1 FINITE-DISCRETE FORMULATION OF APPROPRIATE EQUATIONS

2.1.1 Noise Prediction

In the previous report it was suggested that the vari-
ability of the spectral estimates could be reduced by sub-
tracting from the observed waveform an estimate of the noise
component that is based only on the noise preceding the seis-
mic event. In that report the formulation of the noise-pre-
diction operator was based on a continuous representation of
the noise, as this was more convenient for theoretical pre-
dictions. In this section the finite-discrete formulation is
briefly stated. The theoretical content of this section is
well-known in several contexts (see, for example, reference 2).

Let the samples of a stationary Gaussian process be given by n_i. For convenience assume that the rms value of the samples is 1. Then, writing the correlation coefficients as ρ_k

$$\overline{n_i n_j} = \rho_{|i-j|} \qquad\qquad \rho_0 = 1 \tag{1}$$

Considering an estimate of the form

$$\hat{n}_\alpha = \sum_{i=1}^{M} n_{-i} h_{i,\alpha} \qquad\qquad \alpha = 0,1,\ldots,N-1 \tag{2}$$

the problem is to find the $h_{i,\alpha}$ that minimize the mean square error, given by ε_α^2:

$$\varepsilon_\alpha^2 = \overline{(n_\alpha - \hat{n}_\alpha)^2} \tag{3}$$

The parameter M in Equation (2) represents how much of the previous noise waveform will be used in calculating the estimate. In principle, the quality of the estimate should increase with M. In order to keep computation times within reasonable limits, some compromise must be made in choosing M. Furthermore, since there is some question about the actual stationarity of the noise, a value of M that is too large could, in fact, detract from the quality of the estimate. In the calculations discussed below, values of M up to 200 (which represents 10 seconds at the sampling rate of 20 per second used in these calculations) have been used. The parameter N in Equation (2), which represents the number of samples to be predicted, is usually chosen to equal the number of sample points in the time window used for spectral calculations. Typical values for N in these calculations are 64 and 128. Expanding Equation (3), in terms of the expression for the noise estimate given by Equation (2), and using Equation (1) to substitute for the appropriate expectations, yields

$$\varepsilon_\alpha^2 = \overline{(n_\alpha - \sum_{i=1}^{M} n_{-i} \mathbf{h}_{i,\alpha})(n_\alpha - \sum_{j=1}^{M} n_{-j} h_{j,\alpha})}$$

$$= \overline{n_\alpha^2} - 2 \sum_{i=1}^{M} \overline{n_\alpha n_{-i}}\, h_{i,\alpha} - \sum_{i=1}^{M} \sum_{j=1}^{M} \rho_{|i-j|} h_{i,\alpha} h_{j,\alpha}$$

$$= \rho_0 - 2 \sum_{i=1}^{M} \rho_{\alpha+i} h_{i,\alpha} + \sum_{i=1}^{M} \sum_{j=1}^{M} \rho_{|i-j|} h_{i,\alpha} h_{j,\alpha} \tag{4}$$

Taking the partial derivatives with respect to the $h_{k,\alpha}$ and setting these partial derivatives equal to zero yields

$$\frac{\partial}{\partial h_{k,\alpha}} \varepsilon_\alpha^2 = -2\rho_{\alpha+k} + 2 \sum_{i=1}^{M} \rho_{|k-i|} h_{i,\alpha} \qquad k = 1,M \tag{5}$$

$$\rho_{\alpha+k} = \sum_{i=1}^{M} \rho_{|k-i|} h_{i,\alpha} \qquad\qquad k = 1,M$$

The M linear equations given in Equation (5) specify the M values of $h_{i,\alpha}$ that will yield a minimum value of the mean square error. Equation (5) may be conveniently rewritten in matrix form:

$$
\begin{bmatrix}
\rho_0 & \rho_1 \cdots & \rho_{M-1} \\
\rho_1 & \rho_0 \cdots & \\
\vdots & & \\
& & \rho_0
\end{bmatrix}
\begin{bmatrix}
h_{1,\alpha} \\
h_{2,\alpha} \\
\vdots \\
h_{M,\alpha}
\end{bmatrix}
=
\begin{bmatrix}
\rho_{\alpha+1} \\
\\
\vdots \\
\rho_{\alpha+M}
\end{bmatrix}
\tag{6}
$$

Assuming the covariance matrix is not singular, the solution for the h's may be written immediately from Equation (6) in terms of the inverse of the covariance matrix.

$$
\begin{bmatrix}
h_{1,\alpha} \\
\vdots \\
h_{M,\alpha}
\end{bmatrix}
=
\begin{bmatrix}
\rho_0 & \rho_1 \cdots & \rho_{M-1} \\
\vdots & & \\
\rho_{M-1} & & \rho_0
\end{bmatrix}^{-1}
\begin{bmatrix}
\rho_{\alpha+1} \\
\vdots \\
\rho_{\alpha+M}
\end{bmatrix}
\tag{7}
$$

Substituting Equation (5) into Equation (4) yields a relatively simple expression for the minimum mean square error.

$$
\begin{aligned}
\varepsilon_\alpha^2 &= \rho_0 - 2 \sum_{i=1}^{M} \rho_{\alpha+i} h_{i,\alpha} + \underbrace{\sum_{i=1}^{M} \sum_{j=1}^{M} \rho_{|i-j|} h_{i,\alpha} h_{j,\alpha}}_{\sum_{j=1}^{M} \rho_{\alpha+j} + h_{j,\alpha}} \\
&= \rho_0 - \sum_{j=1}^{M} \rho_{\alpha+j} h_{j,\alpha}
\end{aligned}
\tag{8}
$$

In carrying out the noise prediction with actual seismic data, a long sample of noise (typically, two or three minutes) preceding the event is used to estimate the correlation coefficients. Rather than trying to invert directly the (M-dimensional) covariance matrix, which would not be practical in applications, an algorithm due to Levinson [3] is used. By using this algorithm, the $h_{i,\alpha}$ may be calculated for all α of interest. Examples of the resulting values of ε_α are presented in a later section.

2.1.2 Spectral Calculations

Following the notation of the previous report, but writing equations in discrete form rather than continuous, yields

4

$$z_i = a_i[x_i + n_i] \tag{9}$$

where the x_i and n_i are the signal and noise contributions to the observed samples, the a_i form the time window, and the z_i are the samples to be transformed. To date, only rectangular time windows have been used, and scale factors have been chosen so that the a_i may be written as:

$$a_i = \begin{cases} \dfrac{1}{\sqrt{N}} & 0 \le i < N-1 \\ \\ 0 & \text{elsewhere} \end{cases} \tag{10}$$

where N is the length of the time window. The Fourier series based on the z_i is given by

$$Z_k = \sum_{i=1}^{N} z_i e^{-j\frac{2\pi ki}{N}} \tag{11}$$

and the spectral estimates are simply $|Z_k|^2$. By analogy with the previous report (or by direct calculation) the expected contribution of the noise to the spectral estimates, P_k, may be written as

$$P_k = \sum_{s=-(N-1)}^{+(N-1)} (1 - \frac{|s|}{N}) \rho_s e^{-j\frac{2\pi sk}{N}}$$

$$= \rho_0 + 2 \sum_{s=1}^{N-1} (1 - \frac{s}{N}) \rho_s \cos\frac{2\pi sk}{N} \tag{12}$$

where, as before, the ρ_s are the correlation coefficients estimated from a long run of the noise preceding the event. Equation (12) is simply the smoothed periodogram that corresponds to the choice of time window given in Equation (10). Spectral calculations will be presented in this report in the form of plots of $|Z_k|^2$ and P_k vs. k, or frequency.

2.2 PROGRAMMING CONSIDERATIONS

Some programming was necessary in order to carry out the calculations reported in this chapter. Considerable use was made of subroutines available from the Teledyne staff in writing these programs. The subroutine COOL, which calculates Fourier series by means of the Cooley-Tukey algorithm [4] and the subroutine COOLVOLV, which convolves two waveforms by calculating and multiplying their Fourier series and then calculating the corresponding time series, were used extensively throughout these calculations. (Descriptions of these subroutines may be found in reference [5].) For the noise prediction calculations a straightforward implementation of the Levinson algorithm mentioned above was used. This program is

quite similar to prediction subroutines available from Teledyne, but it is sufficiently different that it was easier to write it separately than to modify an existing subroutine. For some of the calculations, high-pass filtering of the seismic record preceded the spectral calculations. To carry out the filtering, a subroutine was written which calculates the (time-domain) impulse response from a desired frequency-domain response. Filtering was effected by using COOLVOLV to convolve the impulse response of the filter with the entire seismic record. For the number of sample points used in these calculations, it was not necessary to segment the waveforms, as suggested for some filtering applications by Stockham [6].

One problem that arose in filtering the noise waveforms was the occurrence of spurious zeroes in the noise waveform. When parity errors occurred in the digital recording of the seismic record, a value of zero was substituted. These spurious zeroes contributed a ringing when the high pass filter was used. The spurious zeroes were removed from the original record by the following simple rule: whenever a zero or a string of zeroes occurred, the polarity of the samples immediately preceding and following the zero(s) was checked; if the polarity changed, it was considered a "legitimate" zero; if the polarity did not change, the zero was replaced by the straight-line interpolation of the surrounding values. The noise-autocorrelation function was estimated by using COOLVOLV to convolve either a two- or a three-minute sample of the noise with itself. Before any calculations were performed, the mean value of the noise was removed from the entire record and the entire record was divided by the rms level of the noise. Thus, for all of the calculations, the noise process had a zero mean and a unity mean square value.

2.3 NOISE PREDICTION RESULTS

The noise prediction calculations discussed in the previous section have been applied to the seismic record containing the surface focus event and also to three other seismic records consisting only of noise. All of these data are from the same seismometer, which is the center element of LASA cluster AO. For the noise-prediction calculations reported here the autocorrelation function was based on a three-minute sample of the noise waveform except for one case in which a two-minute sample was used. From the correlation coefficients, the $h_{i,\alpha}$ discussed above were calculated. The $h_{i,\alpha}$ were then used to calculate the predicted noise during the interval of interest and, together with the ρ_k, to calculate the expected root-mean-square root of Equation (8) above. Figure 1a presents a portion of the autocorrelation function calculated from the noise preceding a large surface-focus event. The predicted rms error, based on this autocorrelation function, is presented in Figure 2 along with the corresponding curve calculated for three other noise samples. The bottom curve in Figure 2 is the one corresponding to the autocorrelation func-
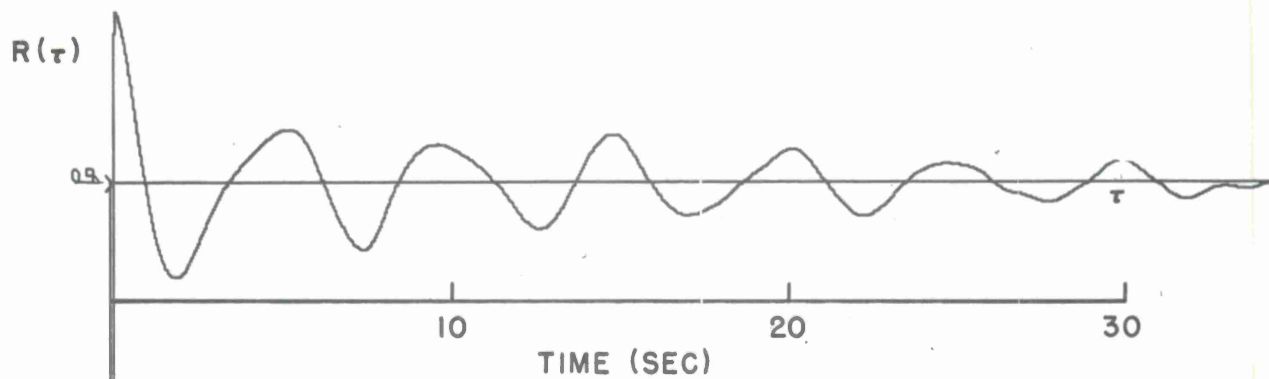
6

FIGURE 1a
AUTOCORRELATION FUNCTION
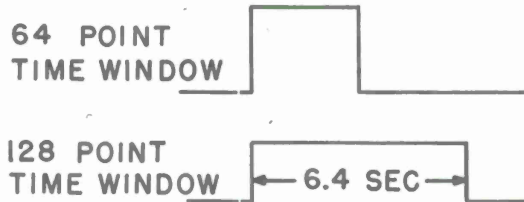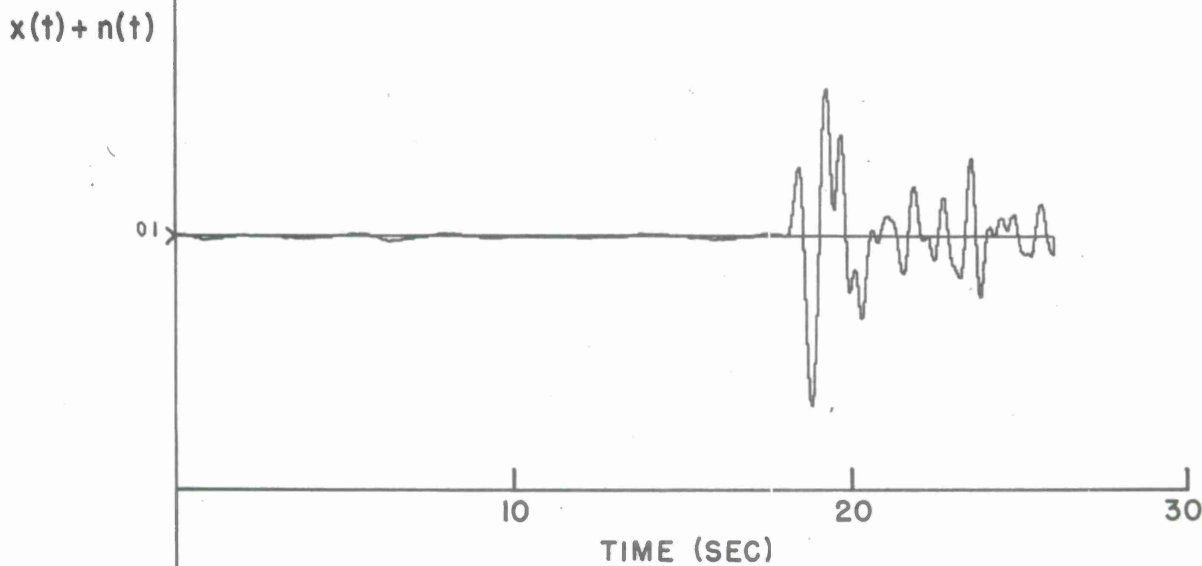CALCULATED FROM 3 MINUTE NOISE SAMPLE

FIGURE 1b
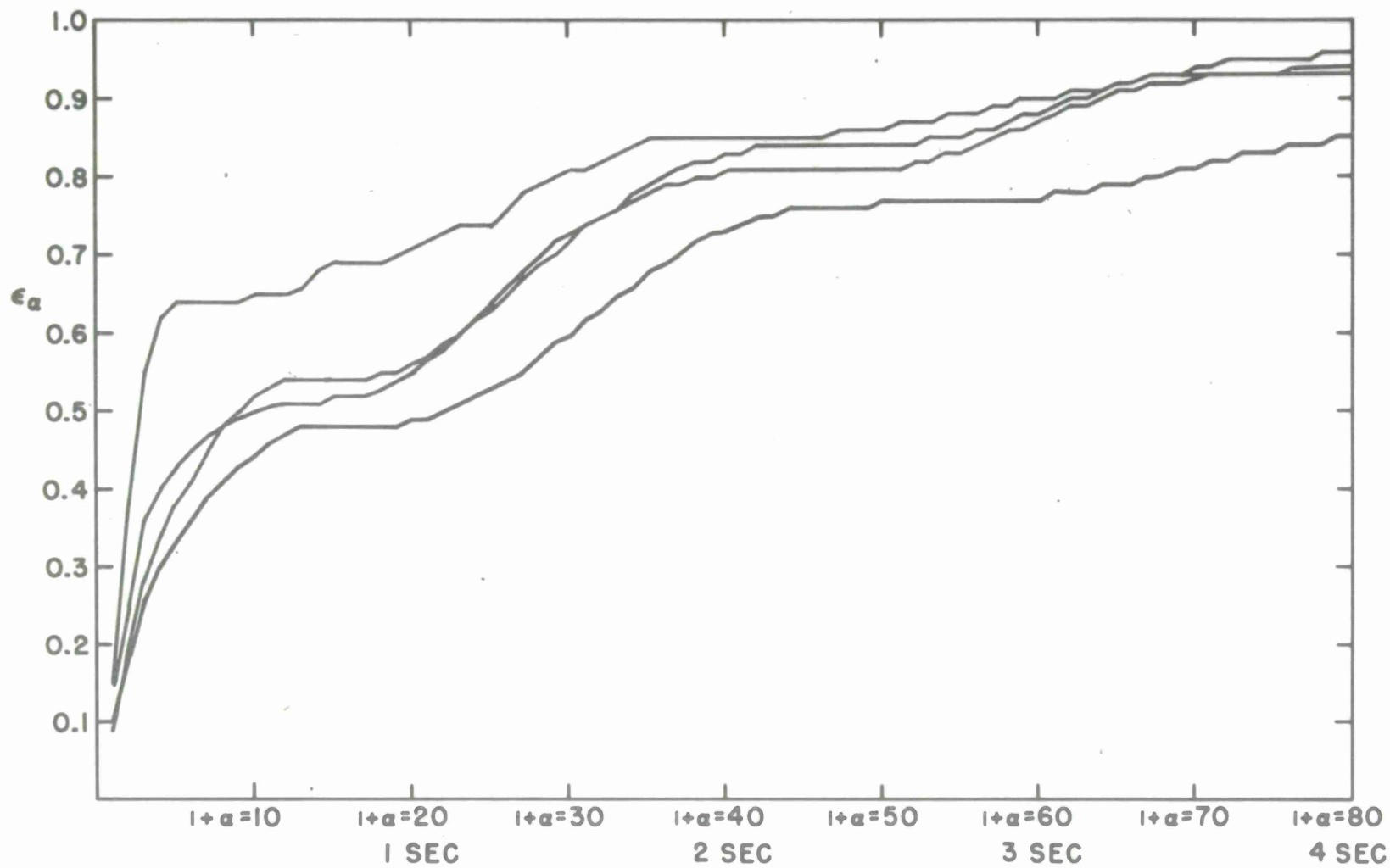SEISMOGRAM OF 13 FEB. '66 EVENT
WITH TIME WINDOWS

7

FIGURE 2

RMS ERROR CURVES

tion of Figure 1a. In all cases the noise is normalized to
have an rms value of 1, so that these curves should asymptote
to a value of 1. For the bottom curve the value at $\alpha = 79$,
which represents a "prediction distance" of 4 seconds, is 0.85.
At one second, the value is 0.49; at two seconds it is 0.73.
The other three curves all indicate a larger rms value at these
times. It is anticipated that the time windows of interest
will be at least three seconds in length. From Figure 2 it
would appear that the noise prediction would significantly re-
duce the rms value of the noise during only a small fraction
of this interval. These calculations have also been performed
on noise waveforms after high-pass filtering. (The details of
the high-pass filter are presented in the next section.) The
resulting rms error curves all were within 90% of their asymp-
totes after one second.

The rms error curve is perhaps the simplest measure of
the quality of the noise prediction. A more appropriate mea-
sure, however, is the reduction in the variability of the
spectral estimate that can be achieved by using the noise
prediction. It seems unlikely with rms errors such as those
of Figure 2 that any significant reduction in the variability
of the spectral estimates would result from using noise pre-
diction. A more direct measure of the value of noise pre-
diction in this context would be a theoretical calculation,
based on the calculated autocorrelation function, of the re-
duction in the variability of spectral estimates as a function
of frequency. This calculation has not yet been performed
with these data, but it is anticipated that this calculation
will show the noise prediction not to be of much value. On
physical grounds it would be expected that the noise prediction
would reduce the variability of spectral estimates mostly at
the low frequencies. This expectation is confirmed in part
by the rms error calculations for the high-pass filtered noise.
The only calculations performed to data that directly reflect
on this question are calculations of the spectrum of 64 and 128
point noise samples with and without noise prediction. As
would be expected from theoretical considerations, the results
of these calculations are highly variable. A quick review of
these calculations suggests that the noise prediction may reduce
the variance of the spectral estimates by as much as one-half
at low frequencies but only negligibly at higher frequencies.
Based on these preliminary calculations it is anticipated that
noise prediction will not be of value in reducing the varia-
bility of spectral estimates.

2.4   RESULTS OF SPECTRAL CALCULATIONS

The seismic event used in these calculations is a large
surface focus event that occurred on 13 February 1966. (PDE
Card No. 9; Epicenter: 49.8N, 78.1E; Magnitude: 6.3; Time:
0 4 57.7 GMT). The recording is from the center element of
LASA cluster AO. Before sampling, the seismogram signal was
passed through an aliasing filter which is flat out to 5 Hz

9

and provides 30 dB of attenuation of 10 Hz. A plot of the seismic waveform is presented in Figure 1b and the time window boundaries are indicated. From this plot it is clear that this is a very high signal-to-noise ratio event.

Results of spectral calculations on this event are presented in this section as plots of $|Z_k|^2$ vs. k, or frequency. The appropriate smoothed periodogram (P_k) is also given on the same plot to allow comparisons of signal-to-noise ratio at different frequencies. In viewing these data it should be recalled that the event treated here is a very high signal-to-noise ratio event so that general conclusions about signal-to-noise ratios as a function of frequency would be inappropriate. Two time windows were used in these calculations: 64 points and 128 points. (Integral powers of two were chosen for convenience in using the Fourier series algorithm, but other values could also have been used.) The calculations based on the 64-point, or 3.2 second, time window are presented in Figure 3 and those based on the 128-point, 6.4 second, time window are presented in Figure 4. Because of the normalization used in defining the time window (Equation 10), the vertical scales on these two figures should be comparable. Specifically, the smoothed periodogram of Figure 3 should be somewhat "smoother" than the one in Figure 4, and this appears to be the case. From these figures it is clear that both signal and noise spectra fall off very rapidly with frequency. A principal contributor to this fall-off is the aliasing filters used in recording these data.

These figures indicate a signal-to-noise (power) ratio on the order of 100 at frequencies as high as 3.75 Hz. Since there is very much more energy at low frequencies, there is the possibility that this apparent energy at high frequencies might simply be a result of the sidelobes in the Fourier transform of the rectangular time windows. As a precaution against this possible artifact, the seismic records were high-pass filtered and the calculations repeated. The frequency response, $H(f)$, of the high-pass filter is given by

$$H(f) = \begin{cases} 0 & |f| < 2.5 \text{ Hz} \\ \frac{1}{2}(1-\cos \frac{2\pi(|f|-2.5)}{2.5}) & 2.5 < |f| < 3.75 \text{ Hz} \\ 1 & |f| > 3.75 \text{ Hz} \end{cases}$$

Because the impulse response of the filter is symmetric about the origin in the time domain, the same location of the time window was used with and without filtering. Spectral calculations based on the filtered seismogram are presented in Figures 5 and 6. As before, the smoothed periodogram was obtained by first estimating the autocorrelation function from a long run of (filtered) noise and then calculating the appropriate smoothed periodogram corresponding to the time window. In Figures 5 and 6 there is apparently some signal energy below 2.5 Hz, despite the fact that the frequency response of
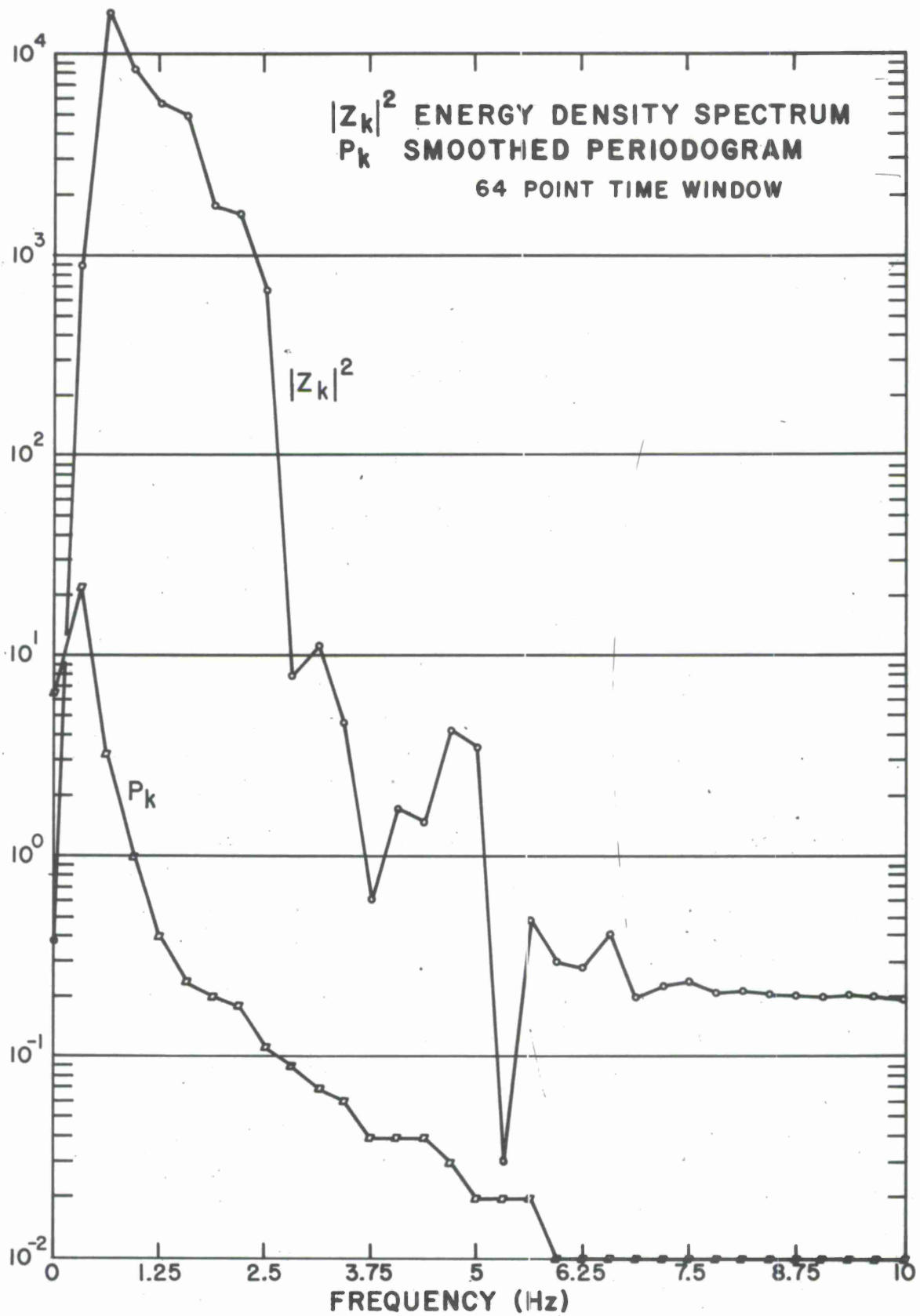
10

FIGURE 3

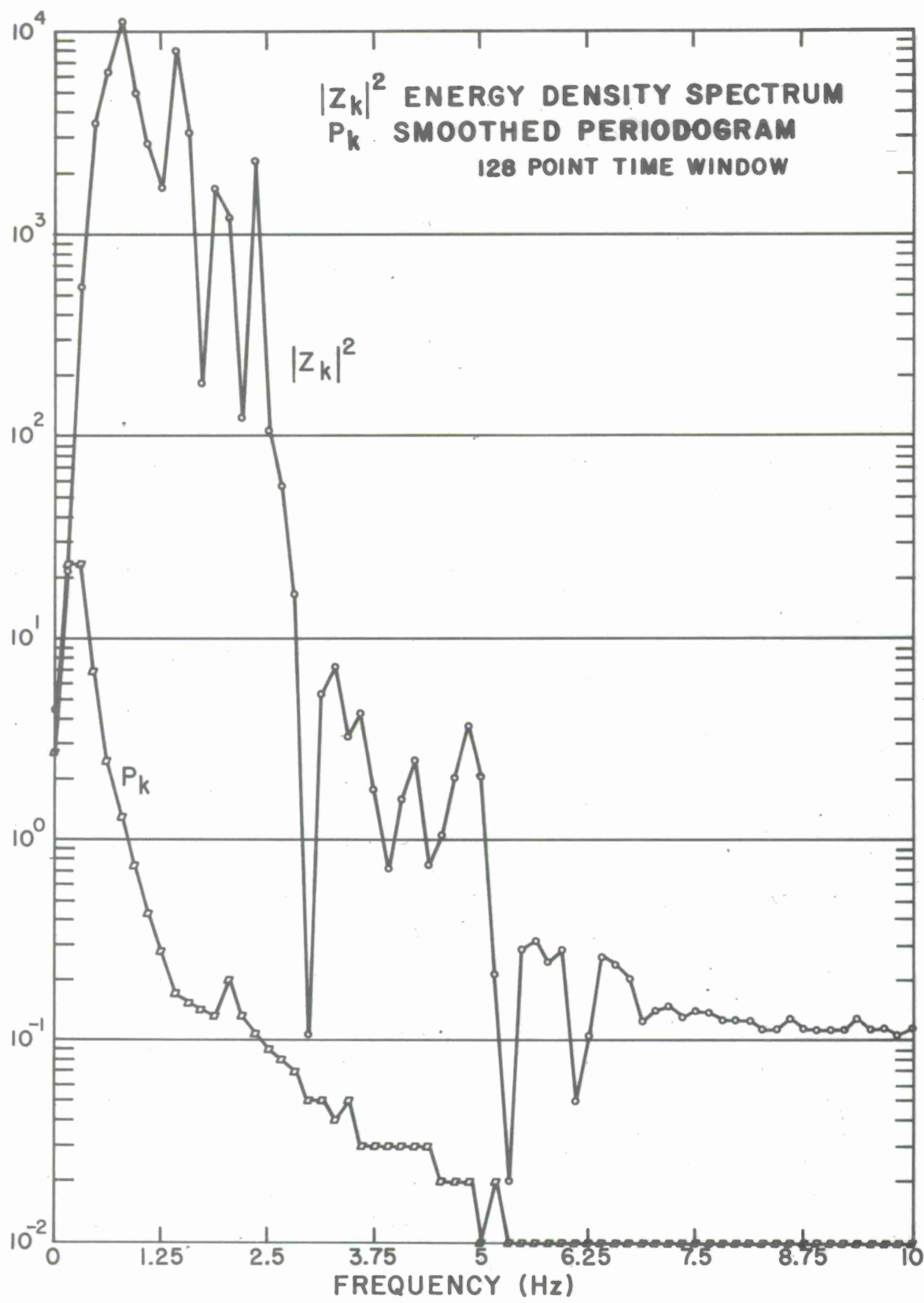64-POINT SPECTRAL CALCULATION--UNFILTERED RECORD
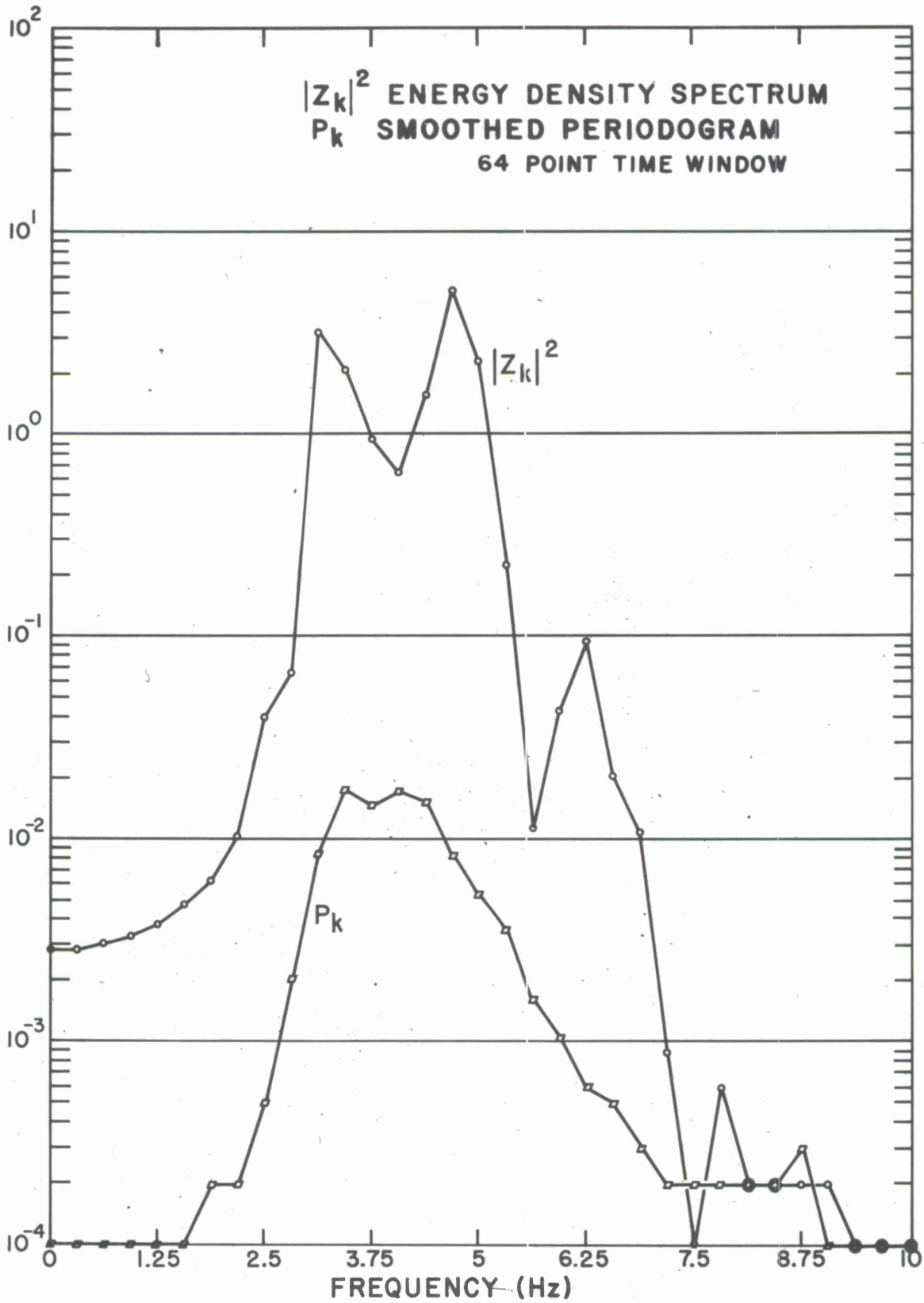
FIGURE 4

128-POINT SPECTRAL CALCULATION--FILTERED RECORD

FIGURE 5

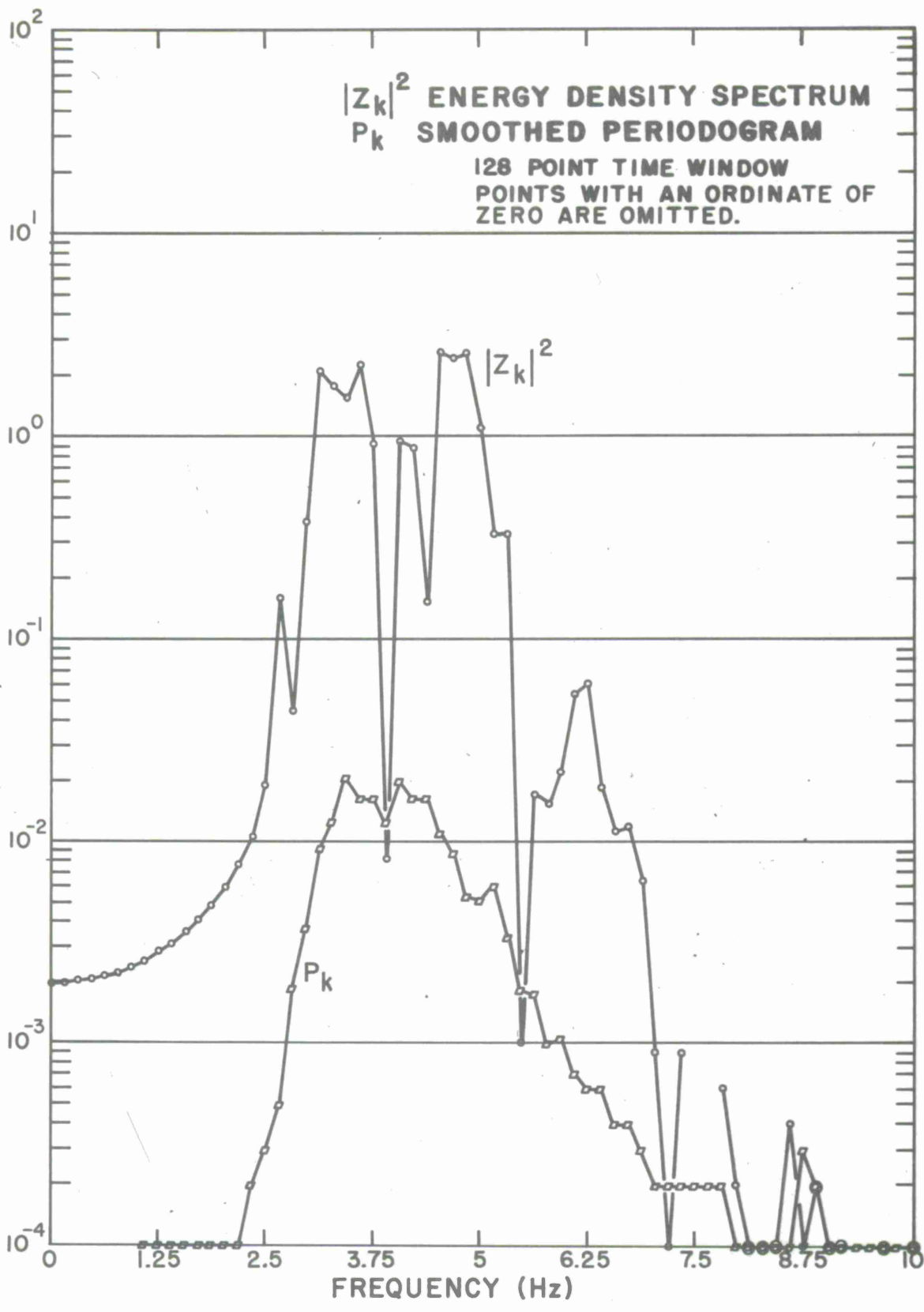64-POINT SPECTRAL CALCULATION--FILTERED RECORD

13

FIGURE 6

128-POINT SPECTRAL CALCULATION--FILTERED RECORD

14

the filter was zero in this region. This is a consequence
of the sidelobe effect mentioned above. It may be observed
from these figures that the good signal-to-noise ratio at
high frequencies is apparently still present. Comparison of
the filtered with the unfiltered spectra indicates that the
spectral levels of the seismic event in the region of 3.75
to 5 Hz are not much affected by the filtering and that, there-
fore, the spectral energy at these frequencies is not a side-
lobe artifact resulting from the low frequency energy. Based
on these calculations it would appear that, for this event,
good signal-to-noise ratios are available at frequencies as
high as 5 Hz. Several qualifications, however, should be
stated with this tentative conclusion. All of the calcula-
tions presented here are based on a single seismic event.
Calculations on several other events would, of course, be
necessary before any inferences about typical spectra could
be made. While it does appear that the high frequency energy
is not a sidelobe artifact, there may be other possible arti-
factual contributors that have not yet been detected. For
example, the data presented in these figures involve a very
large dynamic range. The question of how this range compares
with the dynamic range available in the recording equipment
has not been thoroughly explored.

As a control against possible errors of scale factor,
either in the theoretical formulations or in the programming,
the spectral calculations reported above for the seismic event
were also performed on a control interval preceding the event,
which included only the noise. The filtered record was used
for the examples presented in Figures 7 and 8. As before,
these calculations are presented alongside the corresponding
smoothed periodogram. As discussed in the previous report,
the smoothed periodogram represents the expected value of the
spectral calculation, and the variance of the spectral calcu-
lation at a given point is at least as large as the square of
its expected value, so highly variable results should be ex-
pected from these calculations. This is certainly the case in
Figures 7 and 8. It does appear, however, that the smoothed
periodogram is a reasonable curve for the mean value of the
spectral calculation and, therefore, it would appear that no
serious scale errors were involved in carrying out these calcu-
lations.

One curious similarity between Figures 6 and 8 is the
deep notch in the signal spectrum that occurs just above
3.75 Hz. As the spectral calculation presented in Figure 8
is expected to be highly variable, it may be simply coinci-
dence that a deep minimum in that calculation occurs at the
same place as the deep minimum in Figure 6. However, there
are other possible explanations for this occurrence as well.
Reflections from a subsurface layer near the seismometer
could lead to a series of nulls in the frequency domain. The
seismogram for this event, which was presented in Figure 1b,
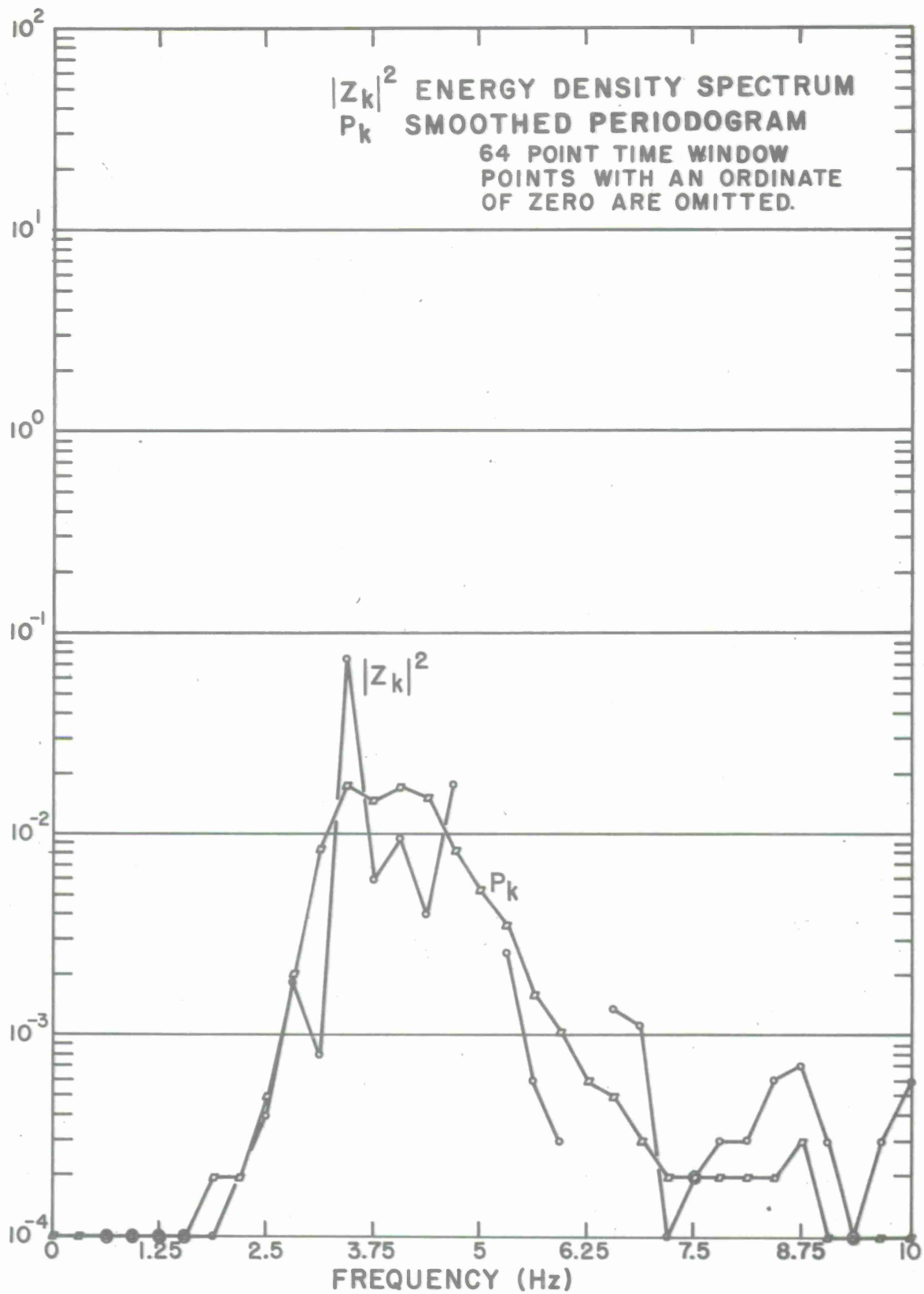suggests secondary arrivals, for example, at 1 and 2 seconds

FIGURE 7

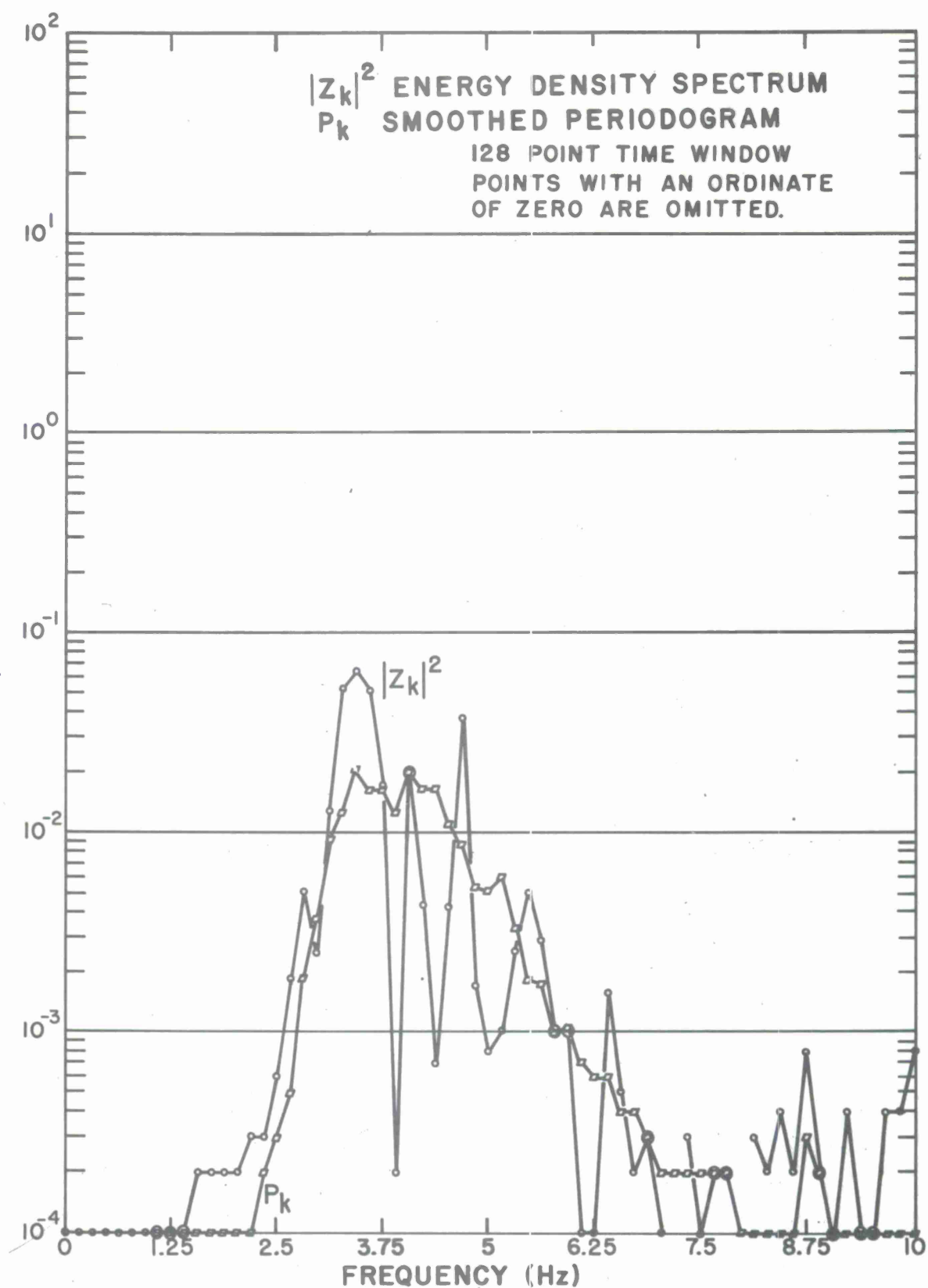64-POINT SPECTRAL CALCULATION FOR CONTROL INTERVAL--FILTERED RECORD

16

FIGURE 8

128-POINT SPECTRAL CALCULATION FOR CONTROL INTERVAL--FILTERED RECORD

17

following the first motion. If the spectral null is due to local conditions, it would be expected that it should also show up in the smoothed periodogram calculated for this noise. (This assumes that a major fraction of the noise energy is distant in origin.) A slight null in the smoothed periodogram at the same frequency does appear in Figure 8. To explore the possibility that this null might have been "smoothed out," another smoothed periodogram was calculated from the same auto-correlation function with four times the resolution of the smoothed periodogram presented in this figure. The results indicated a null at the appropriate frequency at which the smoothed periodogram was approximately one-third of its value at the surrounding points. This result may not be statistically significant, however, since the spectral calculation involved a "maximum lag" of 512 points and the total noise record used to calculate the autocorrelation function was only 2400 points. Similar calculations were performed on other noise records from the same seismometer to see if a null occurred at the same frequency. Although deep nulls do occur in some cases at nearby frequencies, none of them occurred at exactly this frequency.

2.5 CONCLUSIONS

As has already been stressed, the results in this report must be regarded as preliminary. Further calculations on additional seismic events will be necessary before any specific conclusions would be appropriate. Now that the major programming efforts are out of the way, however, it should be relatively easy to perform similar calculations on several other seismic events. Tentative conclusions and plans for continuing this project in the immediate future are given below.

2.5.1 Noise Prediction

From the calculations presented in this report, it does not appear that noise prediction will be a useful tool in estimating the energy density spectrum of seismic events. Before this possibility is discarded, however, a few additional calculations will be performed. If these calculations (which require little further programming) yield the expected results, no further work on noise prediction will be done in this context.

2.5.2 Parameter Choices

The calculations reported above all involve rectangular time windows and only two lengths of these time windows. The questions of what is the best shaped time window and, more importantly, what is the appropriate duration, have yet to be resolved. Additional calculations to be performed on other seismic events will involve the so-called hanning (raised-cosine) window. Eventually the question of optimal window

lengths will have to be studied. The choice of the window
length will, of course, have to be a compromise between the
long window that would yield good resolution in the frequency
domain and a short window that would presumably increase the
signal-to-noise ratio.

2.5.3 Spectral Smoothing to Improve Signal-to-Noise Ratio

The event considered in this report is atypical in that
it has a very high signal-to-noise ratio. In general, it
would be expected that a seismic event might have a good signal-
to-noise ratio at very low frequencies but not at all frequen-
cies. When this is the case, the issue will arise as to how
best to smooth the spectral calculations over frequency in
order to get reliable estimates of the spectrum of the event.
This question was mentioned in the theoretical discussion of
the previous report, where it was indicated that further infor-
mation on the detailed spectra of both the events and the back-
ground noise would be necessary before rules for smoothing
could be developed. It is hoped that some progress on this
topic will be possible as the results of additional calcula-
tions become available.

SECTION III

DETECTION OF NUCLEAR EXPLOSIONS IN THE PRESENCE OF

LARGE NATURAL EVENTS

If a country decided to violate an underground test
ban treaty, one of the strategies it would be likely to
choose is selecting an area of high seismicity for the test.
There are two reasons for such a selection: the nuclear
test might not be detected at all if its signal arrives at
the monitoring stations simultaneously with a large earth-
quake, and, if it is detected it might be mistaken for an
earthquake.

Large events produce signals of considerable duration
at the receiving instruments. A magnitude six earthquake,
for example, is likely to last many minutes before its power
decreases by the equivalent of one magnitude unit. This
slow decay rate of the power at the receiver is the princi-
pal factor that limits monitoring capabilities. Certain array
and signal processing techniques can be used to effectively
reduce the interference of the earthquake. It is the purpose
of this chapter to describe some of these techniques, and
also to report results of their application to date.

The two techniques for suppression of earthquake signals
that are considered here make use of the directional charac-
teristics of arrays. In one case, one or more nulls of the
array pattern are steered in the direction of signals from
the interfering earthquake. The limitations that these nulls
impose on searching nearby regions for test explosions will
be discussed together with the quality of nulls which can be
obtained. In the second case, the efficacy of steering the
main lobe to search for test explosions in the vicinity of the
earthquake - suppression of the earthquake signals to be
accomplished by the sidelobes of the array - will be consider-
ed. In both of these approaches four considerations are of
interest: the relative magnitudes of the two events, the
relative geometry of the two, the relative time of occurence
of the two, and the gometrical distribution of receiving
stations about the epicenters of the two events.

Before proceeding, it should be noted that the second
approach to suppression of the earthquake signals (which
requires a narrow beam and a low sidelobe level so that an
earthquake near the shot epicenter would not contribute sig-
nificantly to the array output when the array is "steered" to
the shot) requires very large arrays for any chance of success.
The 3 dB beamwidth of LASA Montana, for example, is on the
order of 10° at teleseismic ranges - far too large for the
purpose intended here. Thus, continental-sized arrays would
be necessary in order to search for test explosions detonated

20

in seismically active areas. The initial problem in studying this technique is one of obtaining data in suitable format. We have selected events and stations, and requested analog-to-digital conversions of these records for computer processing; only one earthquake has been processed to date.

The bulk of the effort during this period was devoted to the "null solution" to the problem, the remainder of this chapter consists of a discussion of this approach. We shall, in order, consider the near field and teleseismic patterns of dipoles of seismometers, and the effect of a combination of such dipoles into an array of LASA dimensions. Also discussed will be the effect of time sampling rate on the effectiveness of a nulling array, and attempts to remove coda reverberations which represent leakage signals from energy trapped within reflecting layers.

3.1 NEAR FIELD RESPONSE OF SEISMIC DIPOLES

A pair of seismometers the outputs of which are delayed according to some rule and then subtracted, will be referred to a seismic dipole. Let us consider such a dipole as is shown in Figure 9. The array possesses a null in the direction $\theta = 0$ (broadside). The angle θ_m where the dipole response is maximum is given by:

$$\theta_m = \sin^{-1}\left(\frac{1}{2}\frac{\lambda}{d}\right) \qquad \begin{array}{l}\lambda = \text{fundamental wave-} \\ \text{length } (\sim 14 \text{ km})\end{array}$$

We can see that a seismic dipole of length, d, of approximately 60 km would possess a first maximum in its output for an angle, θ, as close as 7 degrees to the null. This high slope of the pattern can be of great help in the problem we are analyzing.

If we choose a delay τ so as to have a null in the direction θ_0, the angle θ_{m_1}, (angle of maximum output, closest to θ_0), will be given by

$$\theta_{m_1} = \sin^{-1}\left(\pm\frac{\lambda}{2d} + \sin\theta_0\right)$$

There are many angles where the conditions for maximum output are satisfied, and they are given by the general expression

$$\theta_{m_j} = \sin^{-1}\left(\pm\frac{2j+1}{2}\frac{\lambda}{d} + \sin\theta_0\right) \quad j=0,1,2\ldots.$$

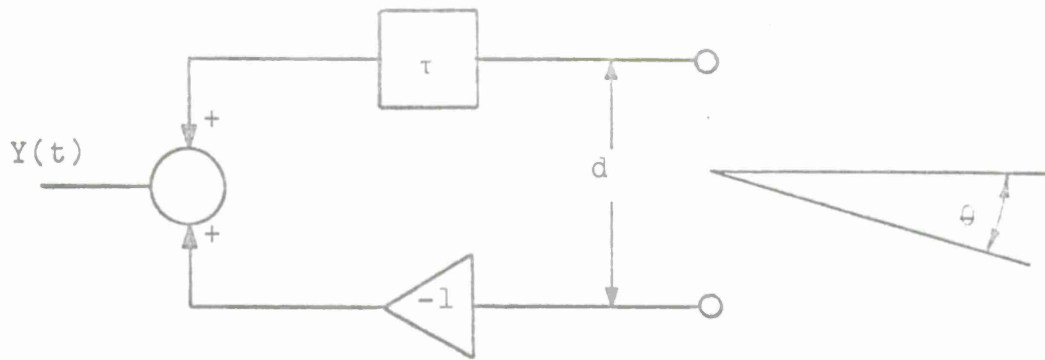The angles for which the output is zero (a null in the pattern) are given by
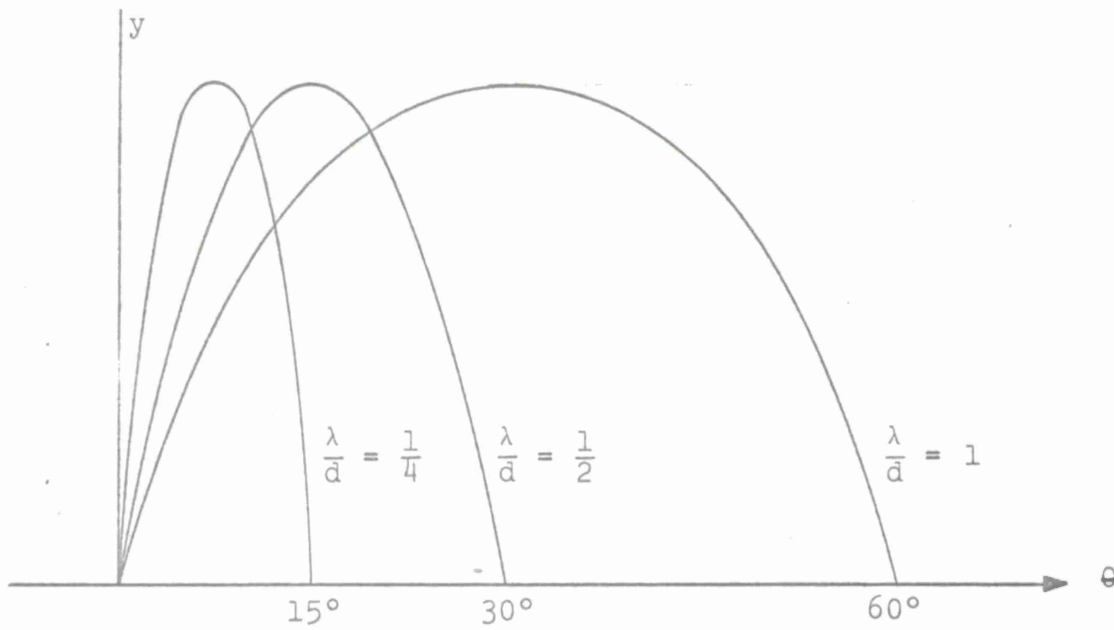
21

FIGURE 9

SEISMIC DIPOLE

FIGURE 10

SEISMIC DIPOLE OUTPUT

22

$$\theta_{n_j} = \sin^{-1}(\pm \frac{j\lambda}{d} + \sin \theta_c) \quad j=0,1,2\ldots$$

The angle θ will be a function of range and azimuth.

The characteristics of the pattern are not greatly affected by the introduction of a delay, the null is just placed at the corresponding θ_0 and for small θ_0, the shape of the pattern will remain very close to the corresponding pattern for $\theta_0=0$ shown in Figure 10.

3.2 TELESEISMIC RESPONSE OF A SEISMIC DIPOLE

Consider a seismic dipole formed with two of LASA's elements. We shall steer a null to a certain point on the surface of the earth and compute the response of the dipole for events coming from the region of the null. Figure 11 presents a schematic diagram of the configuration under consideration.

In order to steer the null to N, we have to introduce a delay τ_0 and then substract the two signals.

$$\tau_0 = k_{\Delta o} \cdot d \cdot \sin\theta_0$$

$$\text{where } k_{\Delta o} = \frac{1}{v}\bigg|_{\Delta_0} \left[\frac{\sec}{\text{degree}}\right] = \text{slope of the travel-time curve}$$

$$d \left[\text{degrees}\right] = \text{length of the dipole}$$

The pattern we expect is shown in Figure 12.

First null:
The locus of the first null is obtained by setting the relative delay between arrivals $= \tau_0$.

$$\therefore d \cdot k_\Delta \cdot \sin\theta = d \cdot k_{\Delta o} \cdot \sin\theta_0$$
(Equation of locus 5 in Figure 12)

The first maximum
In order to have the maximum output, the difference between the actual delay in arrival and the "built in" delay τ_0 should be equal to $\frac{1}{2}T$ where T is the period of the dominant frequency.

$$d \left| k_\Delta \sin\theta - k_{\Delta o} \sin\theta_0 \right| = \frac{T}{2}$$

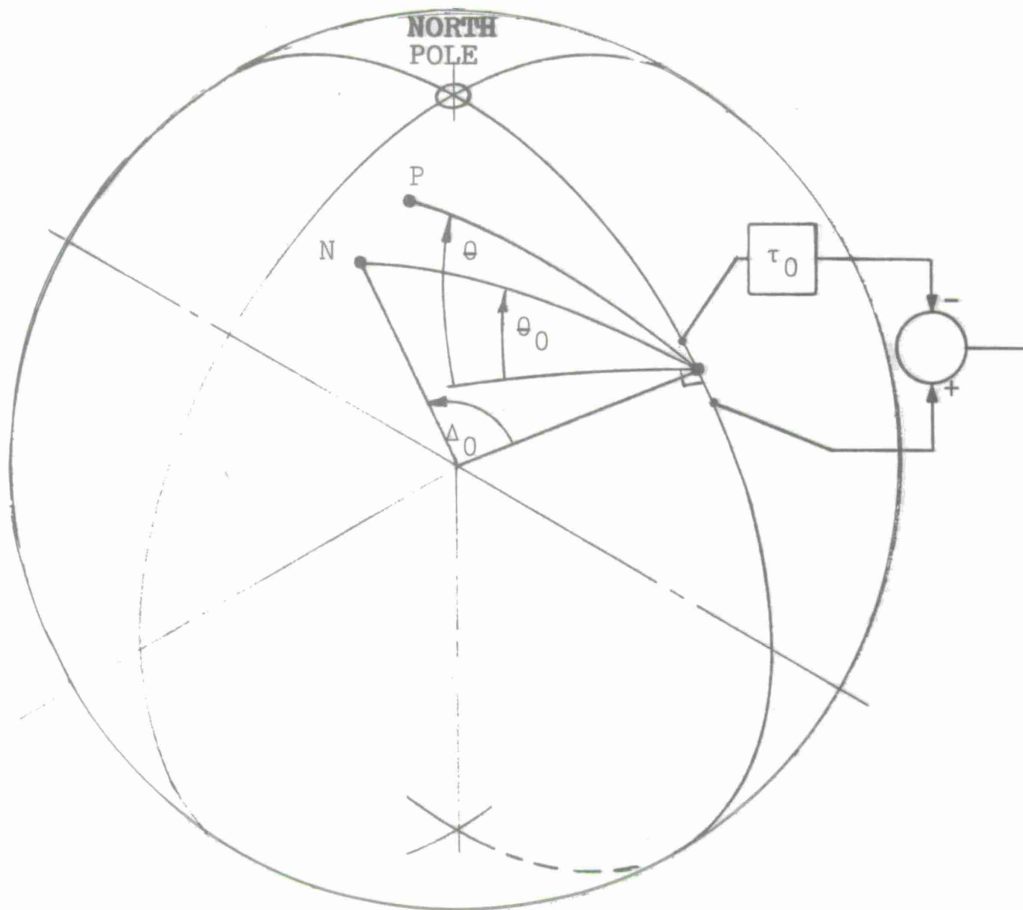In a similar fashion we can find the conditions for the rest

FIGURE 11

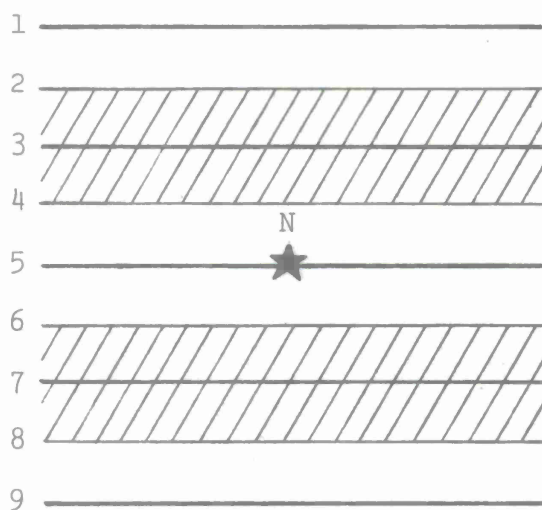SEISMIC DIPOLE LOCATION FOR PATTERN COMPUTATION

FIGURE 12

EXPECTED PATTERN FOR SEISMIC DIPOLE

24

of the contours. The following parameter values were used

$$T = 1 \text{ sec}$$
$$d = 64 \text{ km} = \frac{64}{111.12} \text{ degrees}$$

$$\Delta_0 = 62°$$
$$AZ_0 = 320°$$

The resulting dipole response is plotted in Figure 13; the corresponding region of the total pattern of the dipole is indicated in Figure 14. Observe that if we steer a null at a point O in Figure 14 (broadside to the dipole), then all points lying on the great circle that joins O and the array center, C will also produce a zero response. On the other hand, if we steer the null to a point M (on the axis of the dipole), the great circle joining M and C will show alternating maxima and minima.

The radial beamwidth is considerably greater than the transverse beamwidth for a null placed at M. As a matter of fact, a dipole of approximately 200 km would have the second null at about 20° from the first null.

We can recognize that the response at two dipoles such as shown in Figure 15 is going to show regions of maximum output such as indicated by the shaded areas in Figure 15.

In order to have circular symmetry about the null, N, d_2 needs to be larger than d_1. A distance d_2 on the order of 200 km is required.

We expect that having the freedom to choose elements from a very large array, we can obtain a pattern that has a central null surrounded by a region of high response. The dipoles are required to have different lengths and orientations. Obviously the width of the region of high response depends on the size of the dipoles.

3.3 EFFECT OF TIME SAMPLING RATE ON EFFICIENCY OF NULLING

In order to be able to steer a complete null (- ∞ dB), two conditions have to be satisfied; the signals at the elements have to be identical and the steering delay has to align both signals exactly. The first condition is met fairly well by the first seconds of the P-arrival but not by the P-coda. It was hoped however, that the length of the usable interval might be increased by deconvolution (or some other scheme for removal of reverberation) of the records.

The second condition cannot be met using discrete time records without interpolation, since the desired time resolu-

Shaded regions = All points within 3 dB of maximum
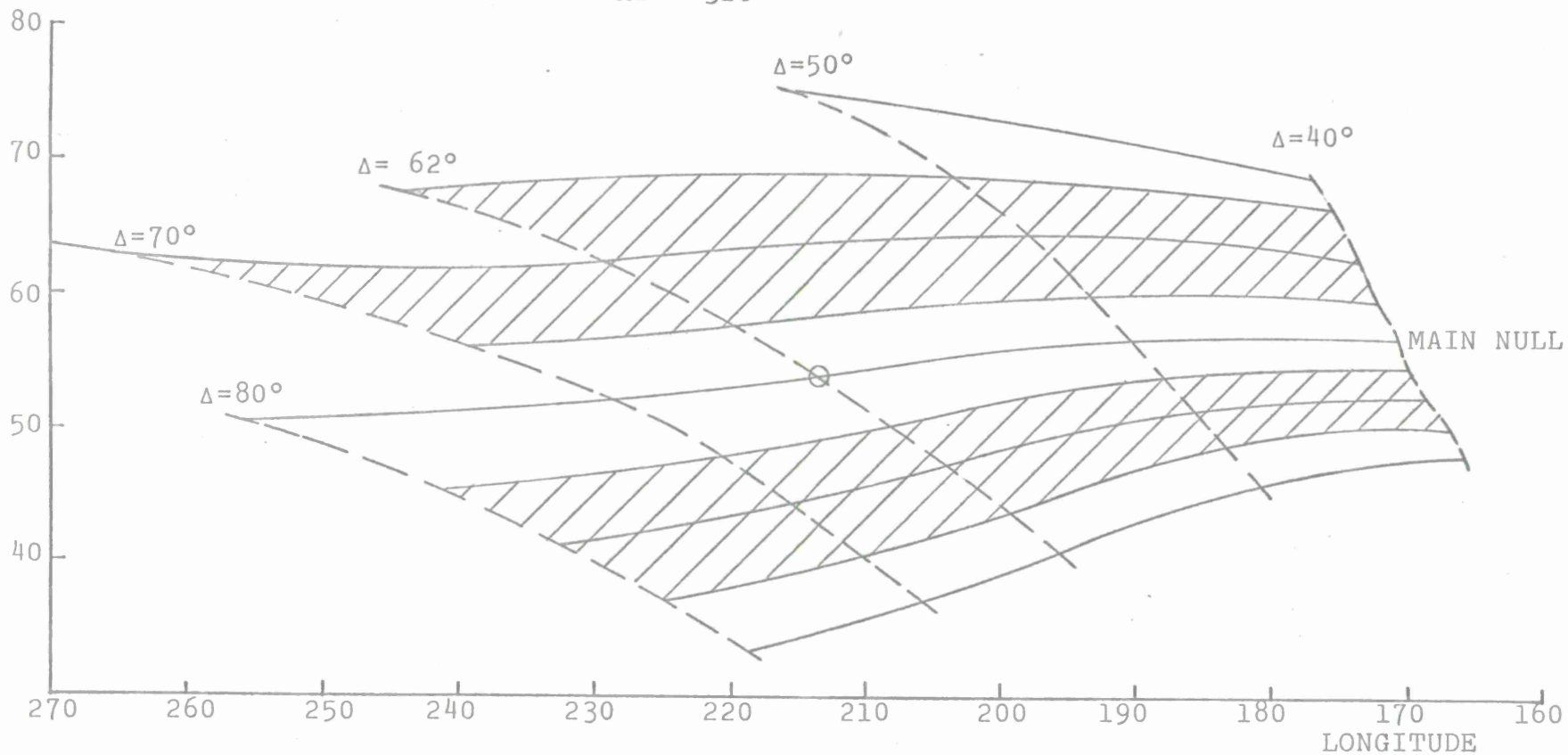
d = 64 km

Location: LASA center

Null coordinates: Δ = 62°

AZ = 320°
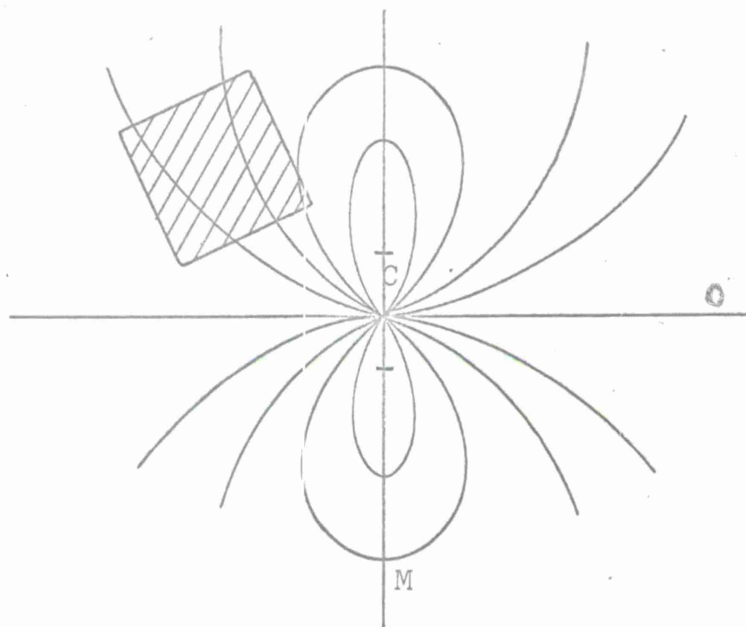

FIGURE 13

DIPOLE PATTERN

FIGURE 14

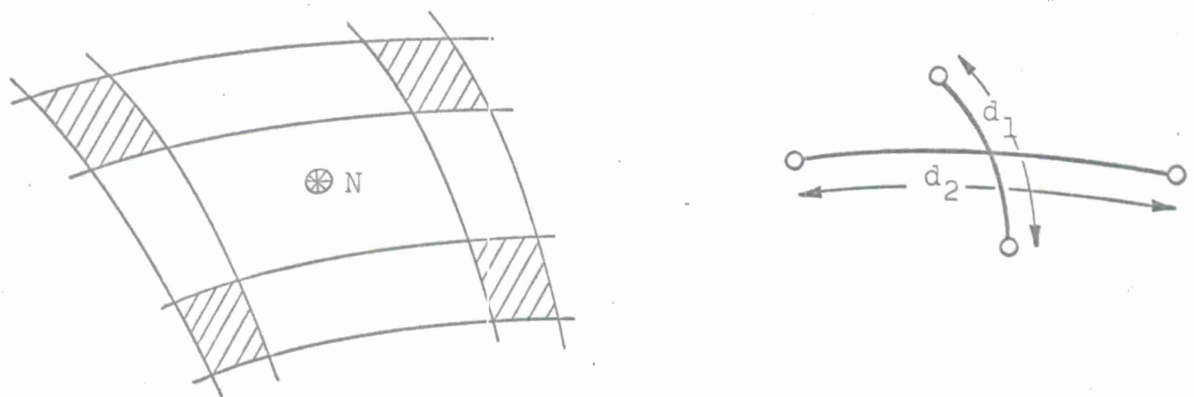REGION OF THE TOTAL PATTERN OF THE DIPOLE
ILLUSTRATED IN FIGURE 13

FIGURE 15

PATTERN OF AN ARRAY OF TWO DIPOLES

tion is less than the sampling period. Using a monochromatic
wave of 1 Hz for illustration, it can be shown that the rela-
tive suppression will be given by:

$$G = \sqrt{2-2 \cos 2\pi\Delta} \text{ where } \Delta=\text{misalignment}$$
in seconds

Three sample values of suppression, corresponding to three
possible values of Δ are tabulated below

$\Delta \begin{bmatrix}\text{Sample point} \\ \text{for 20 s.p.s.}\end{bmatrix}$	$\Delta \begin{bmatrix}\text{Sec}\end{bmatrix}$	G	$G\begin{bmatrix}dB\end{bmatrix}$	$G \begin{bmatrix}\text{Seismic} \\ \text{magnitude}\end{bmatrix}$
0	0	0	$-\infty$	$-\infty$
$\frac{1}{2}$	.025	.155	-16	-.5
1	.05	.285	-10.5	-.3

From this table it is clear that the obtainable suppression
is seriously deteriorated by timing errors. In order to im-
prove the suppression capabilities a higher sampling rate or
an interpolation between the sample points is required.

3.4 IMPROVEMENT IN CODA CORRELATION

As mentioned earlier in this chapter, there is a very
high correlation between the first few seconds of the P-wave
signals received at different receiving sites, even though
these sites may be separated by large distances. It is likely,
then, that a high degree of cancellation of such signals could
be achieved by subtracting one from another after normalization
of the peak values of these signals. P-coda, on the other
hand, is only partly correlated between receiving sites for
signals of shallow earthquake origin ($\rho\approx0.4$) [7] . For shots,
the average coda correlation is close to zero, provided the
receiver sites are separated by at least 100 km. It is hypoth-
esized that there is a correlated part of the earthquake coda
resulting from such things as closely spaced after-shocks, etc.

Since subtraction of uncorrelated signals will not produce
the desired result of lowering the coda energy, attention was
turned towards reducing that part of the coda generated in the
vicinity of the receiver; the hope was that the resulting coda
signal correlation would increase to such an extent that
"nulling" would be a useful tool. As a first step in examina-
tion of this problem, results of Texas Instruments application
of "deconvolution" to several teleseismic events were studied
[8] . This study indicated that the results of these calcula-
tions would not be satisfactory for our purposes. It was con-
cluded that the difficulties are a consequence of the fact that
the two-way travel time in any trapped layer is substantially
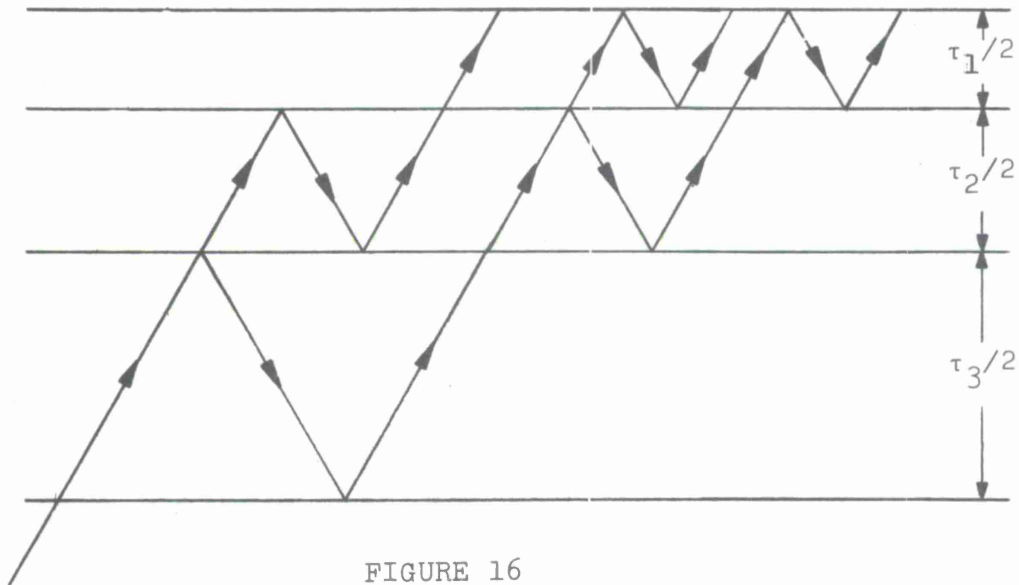less than the duration of the elementary wavelet of the seismic
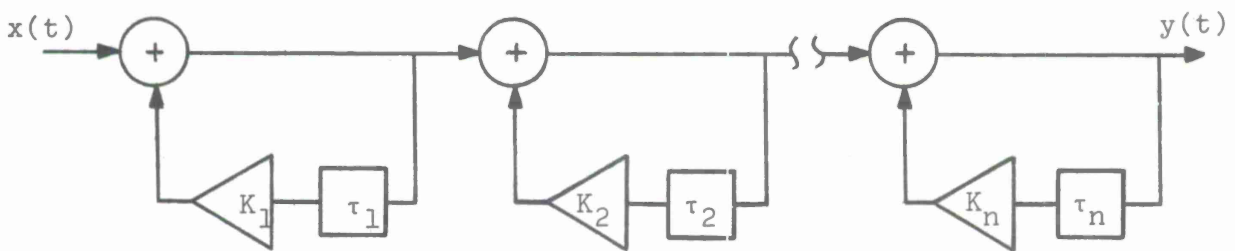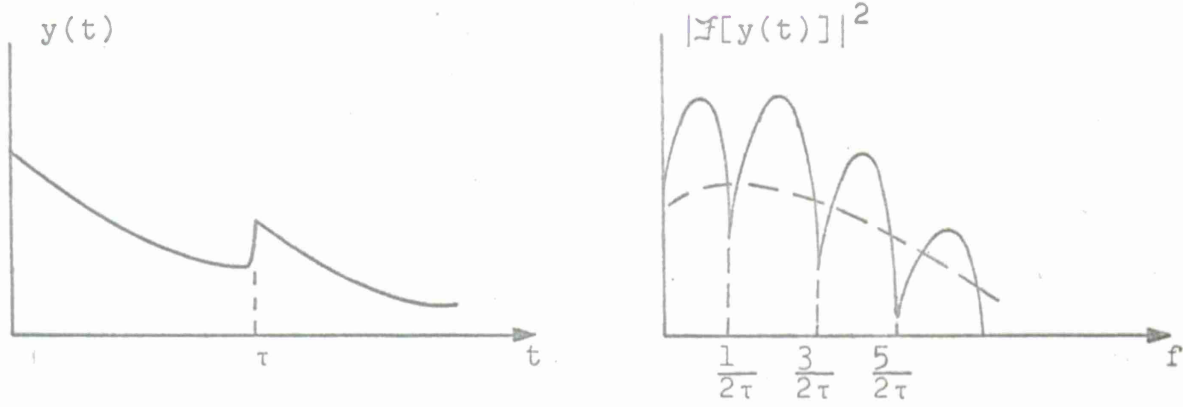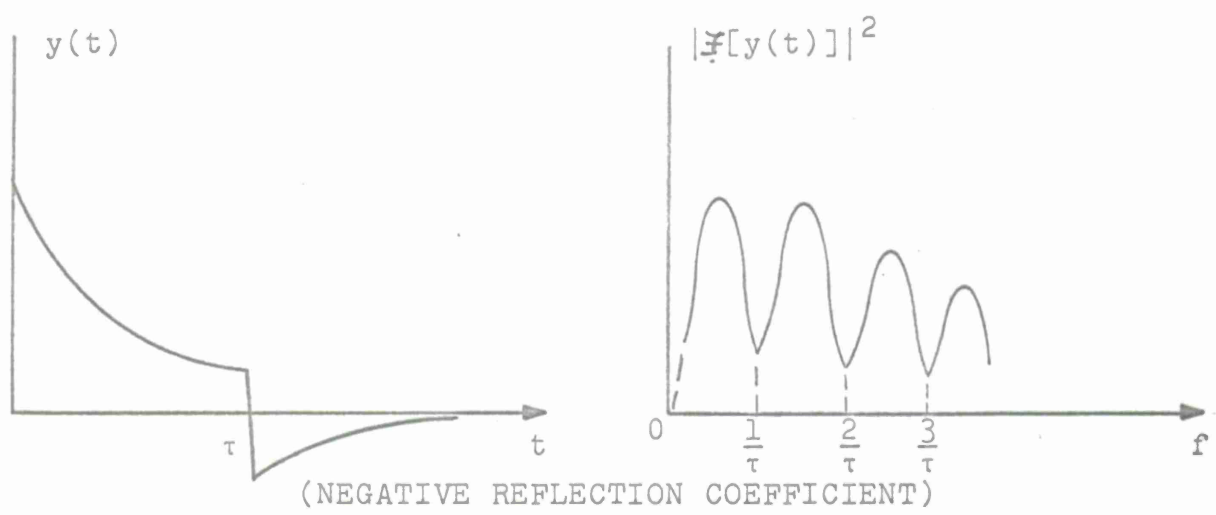signal.

FIGURE 16

MODEL FOR RECEIVING SITE

FIGURE 17

EQUIVALENT FILTER FOR THE LAYERED EARTH

FIGURE 18

RELATIONS BETWEEN DELAYS IN THE TIME FUNCTION
AND MINIMA IN THE ENERGY SPECTRA

In summary, it can be stated that small dipoles (1 or 2 wavelengths) are not useful for the purpose of separating shots and quakes, since the nulls produced by such dipoles cover practically the entire surface of the earth. Further, only a small number of acceptable dipoles can be formed from an array such as LASA Montana. Finally, an interpolation of seismic records between sample times would be necessary if nulling arrays are to be used to solve the overlapping explosion-earthquake problem.

An effort was made to surmount this problem by choosing a different calculation for the removal of reverberation in the vicinity of the receiver. Here, the crust was assumed to be made up of plane-parallel layers, where the trapped signals making up the reverberation are as shown in Figure 16. It was next assumed that the transmission of signals through this crustal model could be represented by a cascade of feedback loops as shown in Figure 17. The delays shown in this figure are equal to the equivalent of the two way travel time within layers, and the loop gains are taken to be the product of the reflection coefficients at the top and bottom of the layers.

If the assumed propagation model were correct, the received signal $y(t)$ would contain sufficient information about the τ's to allow identification of the delays and gains associated with the reflecting layers. Knowledge of these parameters would then permit construction of the inverse filter for the assumed crustal model. This inverse filter would be a cascade of feed-forward loops with gains and loop delays identical with those representing the crust.

3.4.1 Determination of the Layer Delay Times

Where a time function is made up of repeated versions of some wavelet, with even spacings in time, the spectrum of the time function will contain nulls whose location in frequency is related to the time spacing of the wavelets making up the time function. The spacing between these nulls in the spectrum is equal to the reciprocal of the time separation of the wavelets. The frequency of the lowest null is dependent on whether the time function consists of wavelets with all the same polarity (positive reflection coefficients) or consists of wavelets with alternating polarity (negative reflection coefficients). These qualitative observations are illustrated in Figure 18. Of course, with actual events, one expects several reverberating layers. These would produce several sets of nulls in the spectrum of the received waveform, and the various sets would have to be sorted. The sorting problem will be discussed in more detail below.

3.4.2 Determination of Reflection Coefficients

Provided it is possible to determine the delay times associated with the various reverberating layers, the reflection coefficients, or loop gains, may then be determined by passing the time function through a feed-forward loop with time delay equal to the longest observed layer delay. The gain of this loop is varied between zero and one, and the energy in the output observed during a time interval that begins after the onset of the P-wave. The time between the onset of the P-wave and the beginning of this time interval is chosen to be the larger of the following two quantities: the duration of the wavelet and the delay time of the loop. Proper loop gain is that which minimizes this energy. The original time function is passed through the loop with this gain, and the output time function is then passed through a feed-forward loop with the second longest delay time. The process is repeated until all of the delays inferred from the spectrum have been used. The final time function should then have local reverberations removed, and the correlation of coda for two stations should be considerably larger than at the start of the processing.

This processing scheme was checked with a synthetic seismogram. Recovery of the pre-crust waveform was satisfactorily achieved. The next step was application of the technique to the record of an actual seismic event.

3.4.3 Test of the Technique for Removing Local Reverberations

with an Actual Event

To test the computational technique described above on actual data, a surface-focus event (13 Feb. 1966, PDE Card No. 9; Epicenter: 49.8N, 78.1E; Magnitude: 6.3; Time: 0 4 57.7 GMT) recorded at LASA was chosen. This choice was predicated on a number of factors. First, the event was one of large magnitude. Thus, the signal-to-noise ratio was large. Second, as a surface focus event, the seismogram was relatively simple, and the P-coda should be generated almost entirely in the vicinity of the receiver. Finally, the seismogram shows an obvious reflection approximately one second after onset of the P-wave.

The energy density spectrum (based on a 60 sec sample beginning at the first motion) of this event did show many minima and their interpretation in terms of a layer structure was attempted. The first task was to find the delays τ_1 that are consistent with the minima found. For this purpose a program was written which computes the expected minima (for positive and negative reflections) for τ's between 1 sec and 50 sec. These τ's were formed by a geometric series of ratio 1.02. The number of matches with the experimental minima was determined and three values of delays which showed a high correspondence

were selected: 5.6 sec, 1.24 sec, 1.06 sec. These values
corresponded to assumed positive reflections. All attempts
with feed-forward loops to determine the reflection coefficients
of the three layers met with failure, as no minimum energy was
obtained for any gain within the extremes of one and zero.

SECTION IV

LOCATION OF EPICENTERS BY BEAMSPLITTING WITH A LASA

Traditional seismology provides a technique for the
approximate determination of the epicenter of a large event
from the records available at a single seismic station. This
method, first used by Galitzin [9], entails determination of
the station-epicenter bearing from the P-wave onset signals
from a three component seismometer, and the determination of
station-epicenter range from the differential arrival times of
the P and S phases from the event. Unfortunately, this tech-
nique was of limited use, since the S phase of a teleseism
cannot be identified for events much smaller than magnitude
six. Moreover, the precision of bearing determination with a
three component seismometer is on the order of several degrees.
The advent of large aperture seismic arrays offers the possibi-
lity of overcoming both of the shortcomings of the Galitzin
method, and in fact, making possible relatively precise epi-
centeral determinations from a single seismic station.

The way in which a LASA makes this possible is through
determination of the direction of arrival of the phase front
of arriving seismic signals, the P-wave in particular. With
an apperture some ten wavelengths in dimension, rather precise
determinations of both the station- epicenter bearing and the
angle of incidence (directly related to station-epicenter
range) can be made. Here it is important to point out the dif-
ference between the resolution and the precision of angular
measurement possible with an array. The resolution of an array,
the angular separation between two sources required before the
array can identify the fact of multiple sources, is limited en-
tirely by the aperture of the array. It is generally taken to
be approximately equal to the beamwidth of the array. This
beamwidth is approximately 10° for an array of the dimensions
of LASA Montana. The precision of angular determination possi-
ble with an array, on the other hand, is related to both the
array aperture and the signal-to-noise ratio for the received
signals. In theory, an infinite S/N with the smallest of arrays
would permit infinitely fine angular measurements.

Clearly the degree of precision achievable with a given
aperture and a given S/N will depend on the illumination across
the aperture; however, this effect is weak. For filled arrays
(receiving elements at least every half wavelength throughout
the aperture) and continuous wave, analog signals, it can be
shown that where noise alone is the interference, the mean
error in angular determination is zero, and the standard de-
viation of this measurement is inversely proportional to the
square root of the power signal to noise ratio at the output of
the array [10]. While there are other sources of interference
in the case of a LASA making epicentral estimates, let us first
proceed to discuss the implementation of a computational scheme
to achieve angular measurements with precision near the limit
just discussed.

34

4.1 THE MONOPULSE TECHNIQUE OF BEAMSPLITTING

Consider the output of an array as the array is aimed
successively at various angles when there exists a signal
arriving from one direction. This output would peak when the
array is pointed directly at the incoming signal, and would
fall off as the array was steered away from the signal. This
array pattern is illustrated in Figure 19. In the absence of
noise, one could ideally steer the array in successively finer
steps in the vicinity of the maximum response, and eventually
determine that angle of the signal with any degree of precision
desired. When noise is added to the output of the array, how-
ever, the point of maximum response to the signal is increas-
ingly obscured. Thus other means must be sought to determine
the angle of arrival of the signal.

This problem is one which has been successfully attacked
in the case of tracking radar systems, and the technique devel-
oped is directly applicable to the seismic problem. In radar,
the improvement in angular accuracy over conventional use of
arrays has been called beamsplitting, and the particular tech-
nique of beamsplitting to be discussed here is called monopulse.
The monopulse technique makes use of two beams aimed a small
angle apart. The output of one of these beams is then sub-
tracted from that of the other. If the two beams are identical
in shape, this output becomes zero as the pair of beams is
scanned when the signal is arriving at an angle midway between
the two beams. Here the slope of the array pattern, rather
than being zero as it is for the single array being scanned
past the signal, has a relatively steep slope. Thus it is far
easier to implement automatic detection of the zero crossing of
the array output, and hence the angle of arrival of the signal.

4.2 SOURCES OF INTERFERENCE SPECIFIC TO THE LASA PROBLEM

In addition to the noise problem discussed above, there
are several additional aspects of the seismic problem which
will introduce errors in the determination of angles by the
monopulse technique. Most important of these is the fact that
there exist local travel-time anomalies within the aperture of
the array. At LASA these anomalies have been found to be
functions of both the bearing from which the signals arrive as
well as the range between LASA and the epicenters of the events.
These anomalies have been found to be as great as several tenths
of a second [11]. This magnitude of potential time errors makes
it quite difficult to form beams at all, let alone to take pre-
cise measurements of arrival angles from the difference of two
beams. Two separate approaches are being taken to attempt re-
moval of these travel-time anomalies from records for processing.
First, where the S/N is large enough, these anomalies are mea-
sured from the seismic records themselves, and second, where
this is not possible, the average of anomalies from events pre-
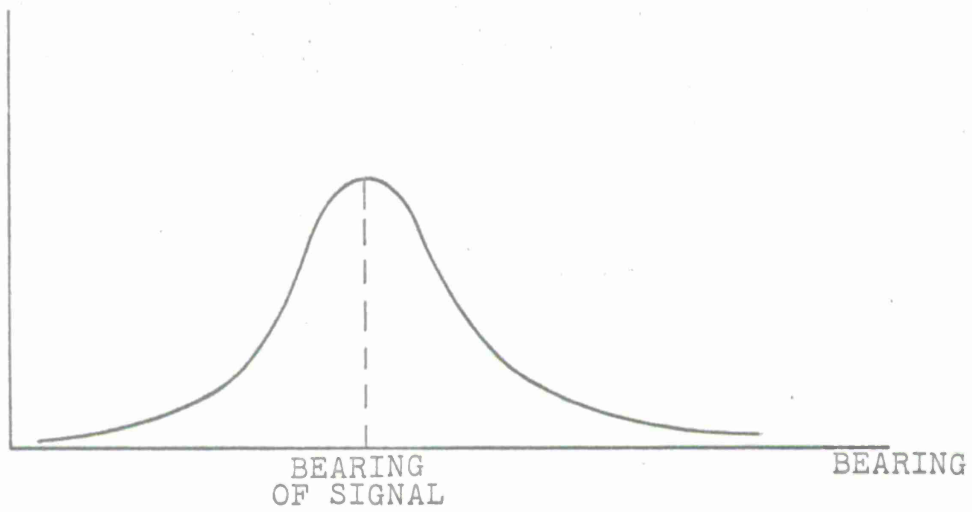viously measured for the particular area are used. For the

FIGURE 19

ARRAY RESPONSE TO A SINGLE INPUT SIGNAL

moment, both methods are being used for large S/N events and the results compared. Not enough statistical evidence is available at this time to predict the magnitude of errors likely to result from these travel-time anomalies.

In addition to the travel-time anomalies discussed above, the time-sampled nature of LASA signals introduces a form of quantization noise in the beam patterns calculated from actual seismic records. While no new information will be gained from the process, it is planned to interpolate the seismograms so as to have a sample rate of 100 per second internal to the computations. During the period covered by this report, however, this interpolation has not yet been included in the computations.

Another problem associated with LASA monopulse arises from the fact that the array patterns, particularly in the radial cut, are asymmetric. As a result, it is impossible to merely squint the two beams equal amounts from the nominal array bearing and define the event location to be that angle midway between the two beams. For the period covered by this report, asymmetric array patterns are being handled on a manual basis; however, a computer program has been written to automatically provide the proper squint angles for the computer beamsplitting process.

Finally, there are two additional ways in which the seismic monopulse system differs from the simpler radar one. First, and perhaps most important, in addition to travel-time anomalies at the various elements of LASA, there are also amplitude anomalies. Thus, the signal-to-noise ratio at the various elements of the array may differ by as much as 3 or 4 dB. When attempting to achieve the maximum performance with small events, the outputs of the various elements would have to be weighted according to the received signal-to-noise ratios. This would produce changes in the basic pattern of the array which would have to be accounted for in the beamsplitting process. Next, it must be noted that all of the foregoing discussion was based on the fact that all events of interest took place at the surface of the earth. This is clearly untrue, and some provision will have to be made so as to be able to deal with events occurring below the surface.

4.3 ACCURACY VS. PRECISION IN EPICENTRAL DETERMINATION

One theoretical point remains to be discussed before examination of experimental results. This point has to do with the fact that the epicenters determined from a single LASA are subject to gross errors in actual location arising from uncertainties in bulk in the travel times. That is, while the precision with which the event is located might become perfect in the absence of noise and all of the other interferences discussed before, the actual epicenter of the event might lie in

some entirely different place than that determined from the beamsplitting process. As calibration of the bulk travel times of the earth becomes more precise, this difficulty may become negligible.

4.4   EXPERIMENTAL RESULTS

During this period, a computer program was employed which used the center elements of the 21 LASA clusters to study three events. The first of these, for the obvious reason that it was the only event with precise position information, was LONGSHOT (29 Oct. '65; PDE Card No. 89; Epicenter: 51.4N, 179.2E; Magnitude: 6.1; Time 21 00 00.1 GMT). The remaining two events were a Kurile Island earthquake (12 Dec. '65; PDE Card No. 91; Epicenter: 51.5N, 178.9W; Depth: 50 km; Magnitude: 5.0; Time 00 48 01.7 GMT) and a Semipalatinsk surface-focus event(13 Feb. '66; PDE Card No. 9; Epicenter: 49.8N, 78.1E; Magnitude: 6.3; Time: 0 4 57.7 GMT). At the beginning of this work it was not realized that considerable asymmetry existed for the main lobe of the LASA beam -- particularly in the radial direction. For this reason, the two beams of the monopulse system were squinted equally. That is, for example, in the azimuthal scan one beam was squinted 6° to the right, while the second was squinted 6° to the left. Radial squints for these runs were 3°. In addition, the difference beam out-put was normalized by dividing by the unsquinted beam response. Both of these procedures were found to cause troubles -- shifts in the null position of the monopulse beam and distortion of the difference beam pattern. While it was not considered nec-essary to change the computer program to take care of these problems during this period (asymmetries were estimated man-ually), the program has at this time been modified to auto-matically provide the proper asymmetrical squint by computing the array patterns in the vicinity of the event location.

Figures 20 and 21 show the processed array outputs while scanning past the approximate position of LONGSHOT for the azimuthal and radial cases, respectively. As stated above, equal azimuthal squints of 6° and radial squint of 3° were used for this computation. The J and B surface-focus tables were used for these computations. Total scan for both cases includes 400 steps, each step being two kilometers in range and 0.029° in bearing. Local travel-time anomalies for this mea-surement were determined from the mean value of the anomalies measured for each cluster by Teledyne [11]. The LONGSHOT posi-tion determined from the zero-crossings shown in these figures differs markedly from the true position of the event, approxi-mately 70 km in range and approximately 1.4° in bearing. In addition, the beam response is markedly jagged -- far too much so for the signal-to-noise ratio of the received signals. This latter phenomenon has since been traced to a time-quanti-zation noise (time samples too far apart for the differential type of calculations being used) and will be corrected for in the future by interpolating the seismograms between samples as a part of the beamsplitting process.
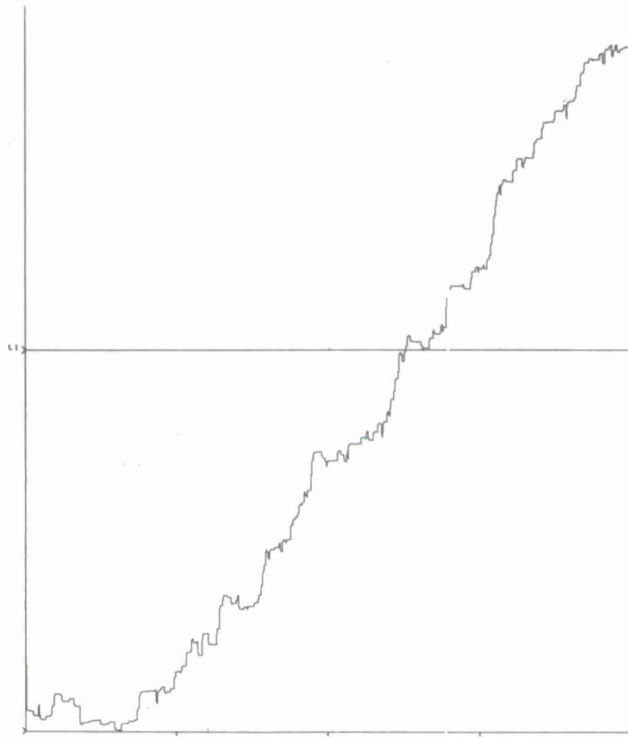
FIGURE 20

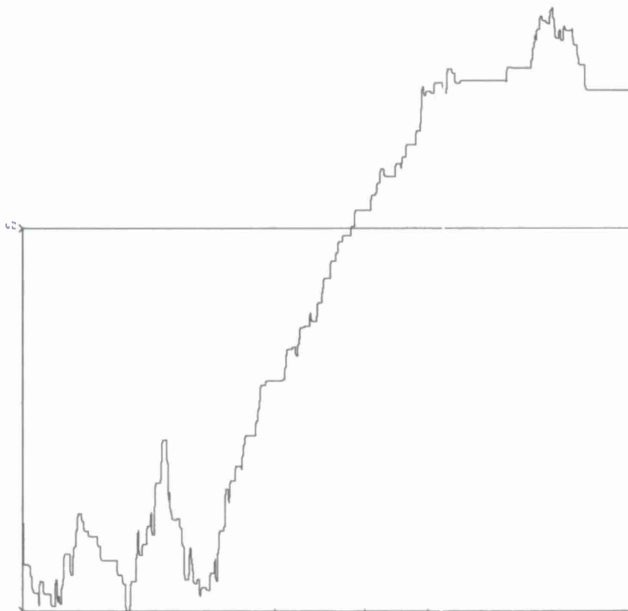AZIMUTH DIFFERENCE PATTERN(LONGSHOT)

FIGURE 21

RADIAL DIFFERENCE PATTERN (LONGSHOT)

In an effort to discover the cause of the location errors of this first calculation, other runs of the LONGSHOT data were made. Figures 22 through 25 give the outputs of one of these runs. The size of the scanning steps for this run are substantially larger than in the previous run (0.143° in azimuth as compared with 0.029°, and 0.180° radially as opposed to 0.018°) to observe gross characteristics of the array patterns. Figures 26 through 29 correspond to the 13 Feb. 1966 event. Figure 26 gives the unsquinted azimuthal scan of the array, Figure 27, the difference beam output for azimuthal scan, Figure 28, the unsquinted radial scan of the array, and Figure 29, the difference beam output for this same scan. One other difference in the computation must be noted. Azimuthal squint for this run was reduced to 3°. The most obvious feature of this run is the asymmetric character of the radial unsquinted beam. A second prominent feature of this same pattern is the existence of a substantial flat in the pattern occurring in the vicinity of the short range 3 dB point.

This asymmetry in pattern coupled with equal squint angles will cause substantial offset in the zero crossing location for the difference pattern for the radial case. In fact, when a manual correction for this asymmetry was applied to the data shown for the preceding run, the 70 km discrepancy between actual and measured range for LONGSHOT was reduced to approximately 2 km. The flat in the pattern, due in part to a relative flat in the travel-time tables for these ranges, suggests that extreme care must be taken in forming difference patterns. While the obvious correction for such conditions is to employ small squint angles, such action will reduce the slope of the difference beam in the vicinity of the zero crossing, and hence lower the precision of the measurement. While the asymmetry of the unsquinted azimuthal beam is far less than that of the radial beam, reduction of the squint angles for the difference beam from six to three degrees halved the discrepancy in bearings between actual and measured. Later refinement of local travel-time anomalies reduced this error to less than 0.1° (using anomalies measured from the LONGSHOT event itself rather than the average anomalies discussed above).

Figures 30 through 33 show the results of one run with the small scan steps for the earthquake. These runs were made using average anomalies from the Teledyne report. As can be seen from the figures, the results of these computations differ widely from the LONGSHOT results. While exceedingly poor azimuthal estimates are possible from these data, no range estimates to the events are possible at all. It was suspected that incorrect travel-time anomalies were responsible for the poor results obtained. As a check of this assumption, the Semipalatinsk event was rerun with the larger scan steps. Results of these computations are shown in Figures 34 through 37. As can easily be seen from these figures, no real beams are being formed. Since the ability to form beams with an array depends critically on good timing information, this lack of proper beam formation suggests strongly that the travel-time anomalies were in fact incorrect.

The results outlined above suggest the directions to be taken in the next period for the problem of beam splitting. First, more accurate local travel-time anomalies must be sought. This will not only include anomalies for the events studied so far, but also average anomalies for several regions under study. Second, time interpolation of seismograms will be included in the computer program to minimize the time-quantization noise described above. Third, automatic asymmetric squinting will be included in the program. Fourth, normalization of the difference beam by the unsquinted pattern of the array will be eliminated. Finally, polynomial fitting of the difference beam to improve estimates of the zero crossings will also be included in the program.

In addition to these corrections to the computational procedure, the number of events studied will be increased with emphasis placed on small magnitude events.
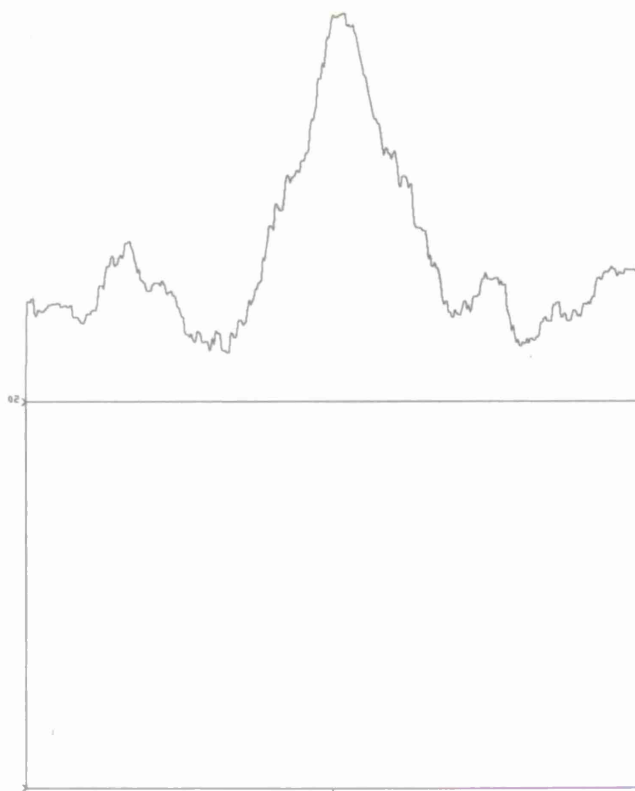
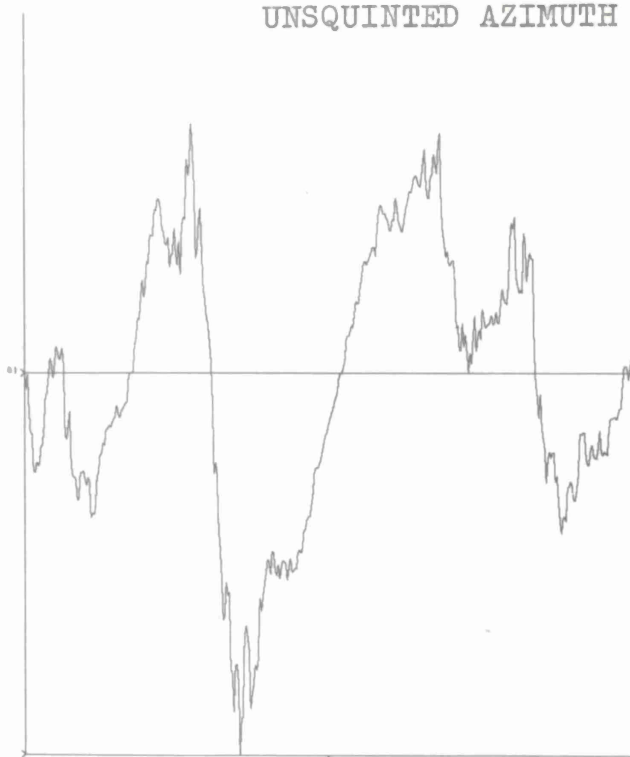FIGURE 22

UNSQUINTED AZIMUTH PATTERN (LONGSHOT)

FIGURE 23

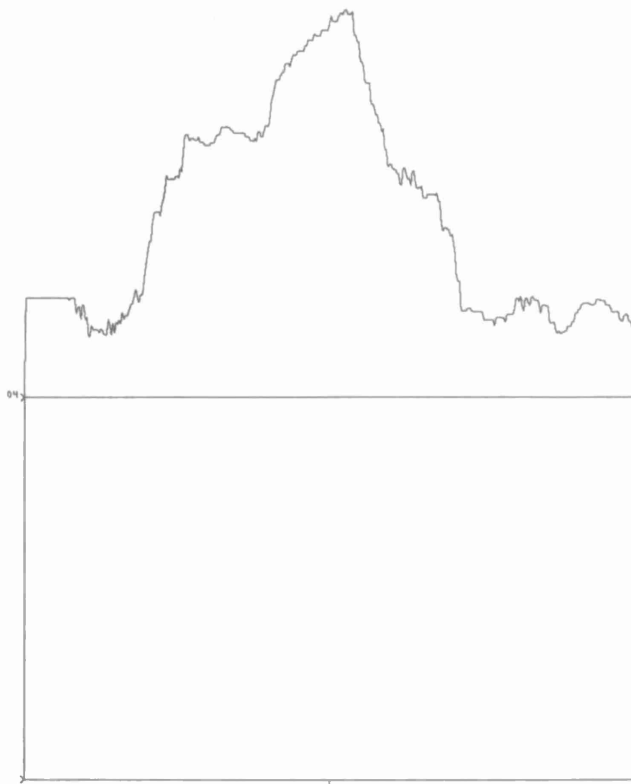AZIMUTH DIFFERENCE PATTERN (LONGSHOT)

42

FIGURE 24
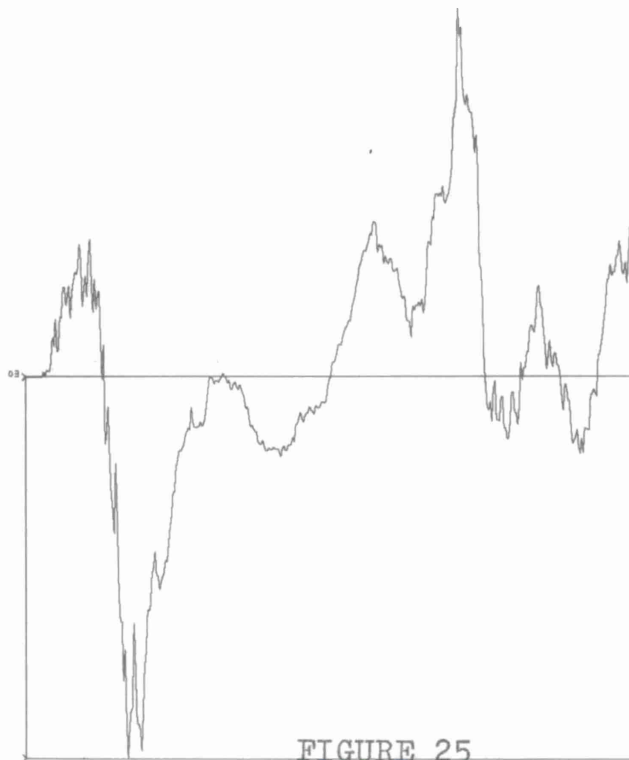
UNSQUINTED RADIAL PATTERN (LONGSHOT)

FIGURE 25

RADIAL DIFFERENCE PATTERN (LONGSHOT)

FIGURE 26

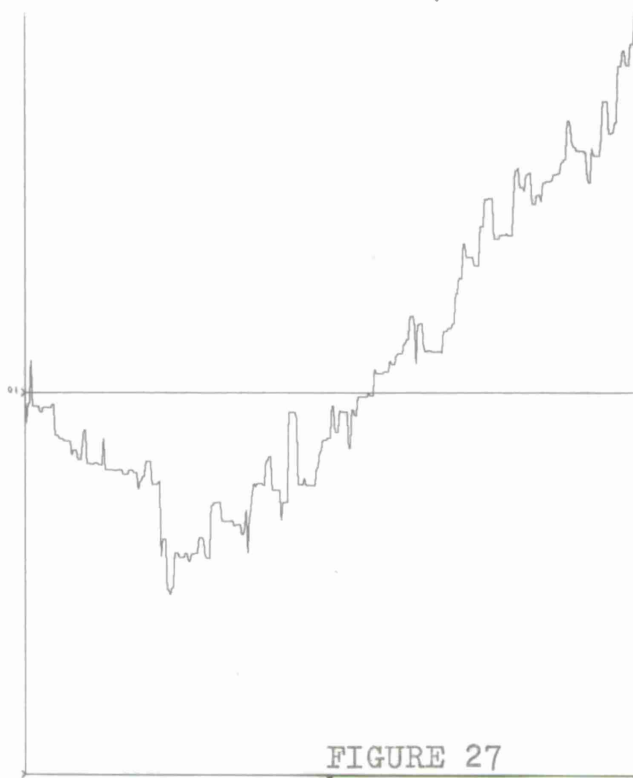UNSQUINTED AZIMUTH PATTERN (SEMIPALATINSK 13 FEB. '66)

FIGURE 27

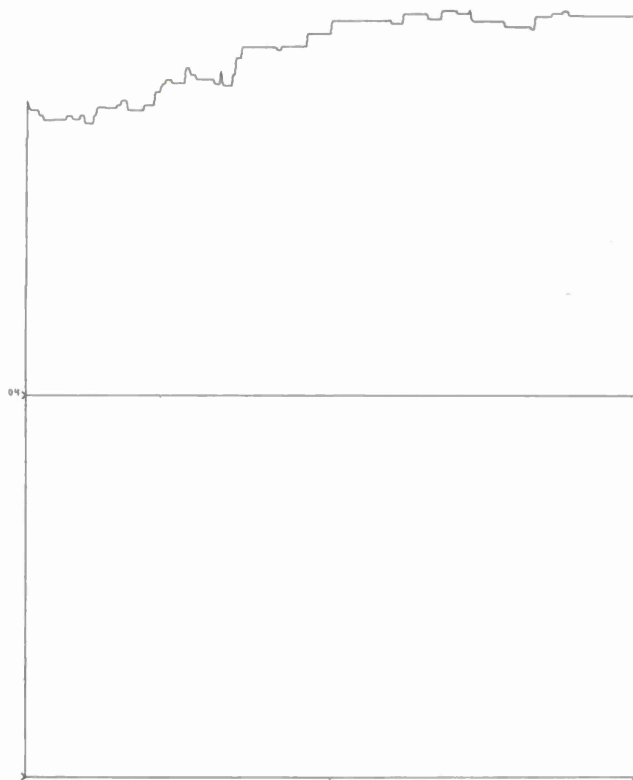AZIMUTH DIFFERENCE PATTERN (SEMIPALATINSK 13 FEB. '66)

FIGURE 28

UNSQUINTED RADIAL PATTERN (SEMIPALATINSK 13 FEB. '66)

FIGURE 29

RADIAL DIFFERENCE PATTERN (SEMIPALATINSK 13 FEB. '66)

FIGURE 30

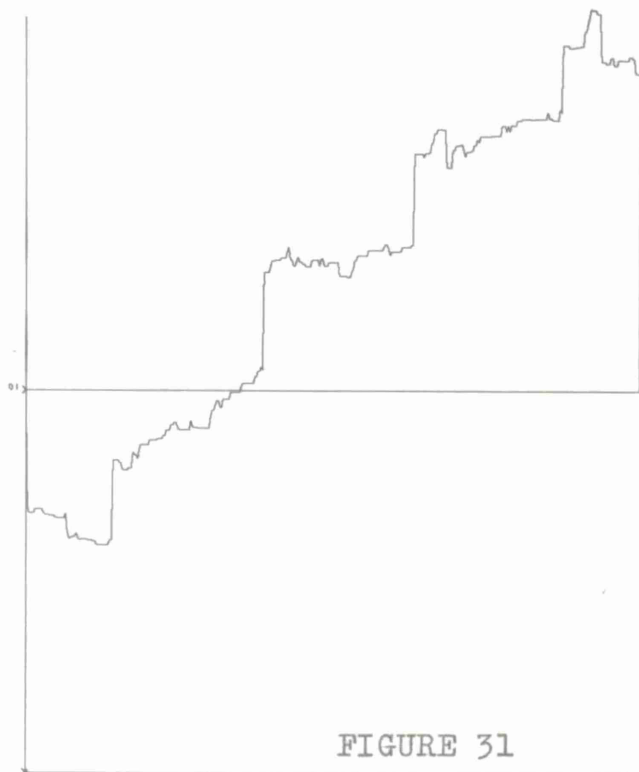UNSQUINTED AZIMUTH PATTERN (E.Q. KURILE IS. 12 DEC. '65)

FIGURE 31

AZIMUTH DIFFERENCE PATTERN (E.Q. KURILE IS. 12 DEC. '65)

46

FIGURE 32
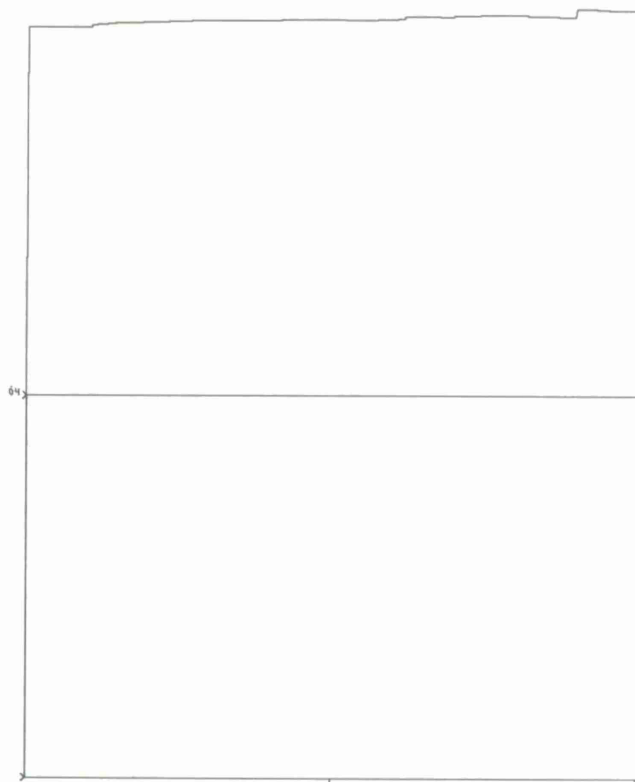UNSQUINTED RADIAL PATTERN (E.Q. KURILE IS. 12 DEC. '65)
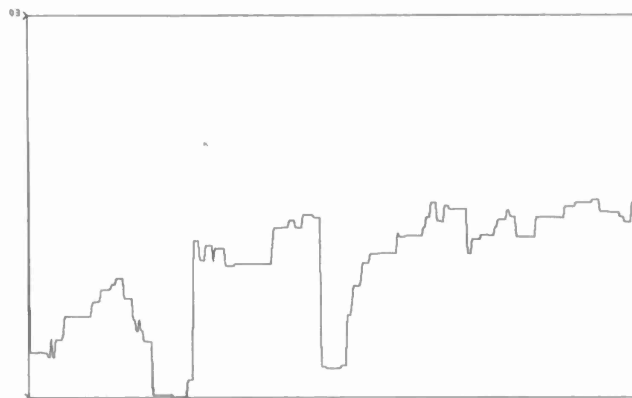

FIGURE 33
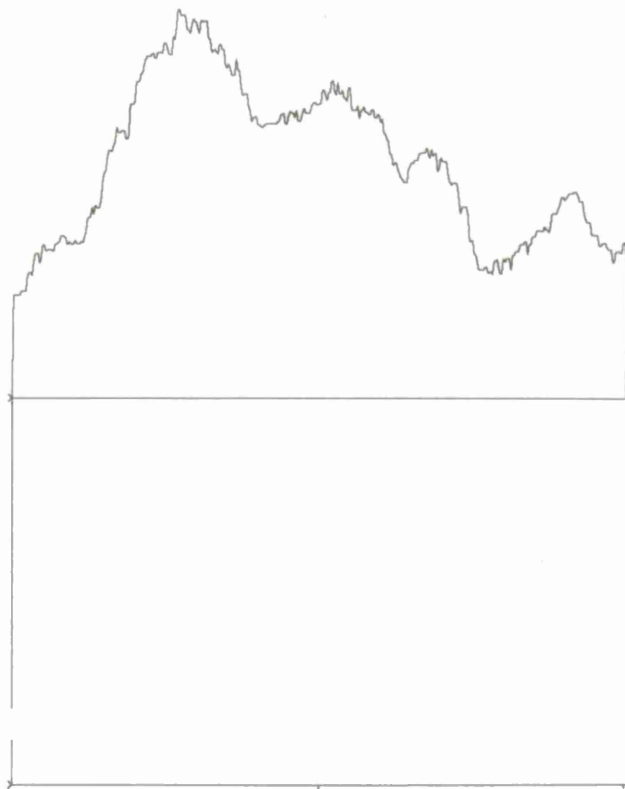RADIAL DIFFERENCE PATTERN (E.Q. KURILE IS. 12 DEC. '65)

47

FIGURE 34

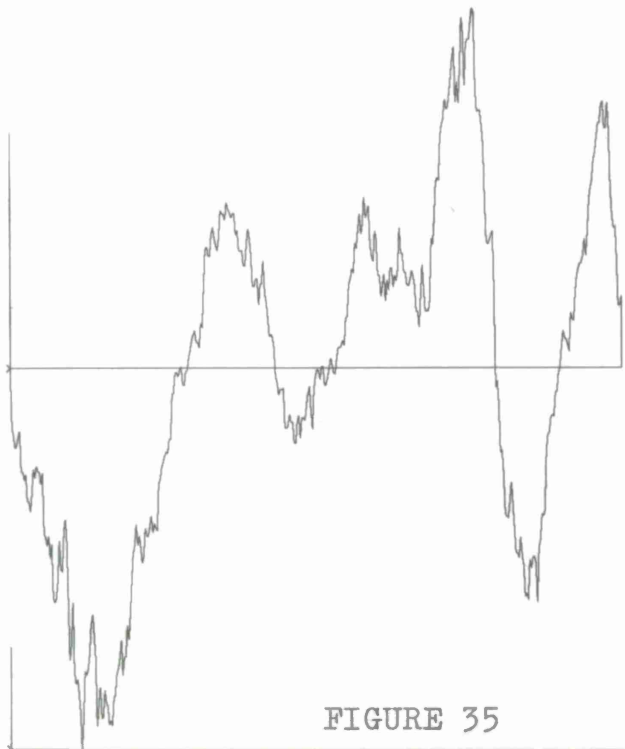UNSQUINTED AZIMUTH PATTERN (SEMIPALATINSK, FEB 13 '66)

FIGURE 35

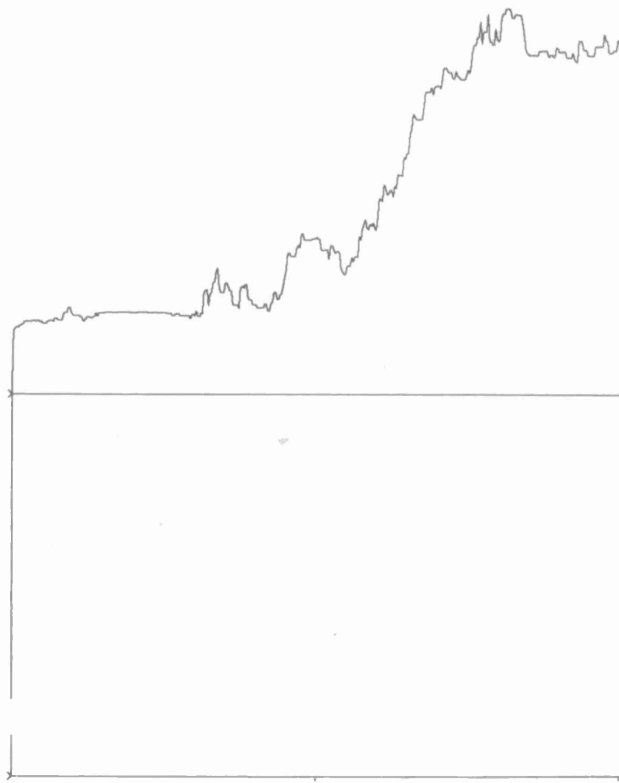AZIMUTH DIFFERENCE PATTERN (SEMIPALATINSK, FEB. 13 '66)

FIGURE 36
UNSQUINTED RADIAL PATTERN (SEMIPALATINSK, FEB 13 '66)

FIGURE 37
RADIAL DIFFERENCE PATTERN (SEMIPALATINSK, FEB 13 '66)

49

REFERENCES

1. "Second Quarterly Technical Report on Large Aperture Seismic Arrays," General Atronics Corp., February 1967, Contract AF19(628)-5981.

2. H. Cramér, *Mathematical Methods of Statistics,* Princeton University Press, Princeton, 1954, pp. 302-305.

3. N. Levin, "The Weiner RMS (Root Mean Square) Error Criterion in Filter Design and Prediction," *J Mathematics and Physics*, vol. XXV, no. 4, January 1947, pp. 261-278, reprinted in Appendix B of N. Wiener, *Extrapolation, Interpolation, and Smoothing of Stationary Time Series,* Technology Press, Cambridge, 1949.

4. J.W. Cooley, J.W. Tukey, "An Algorithm for the Machine Calculation of Complex Fourier Series," *Mathematics of Computation,* vol. 19, no. 90, pp. 297-301, April 1965.

5. D.W. McCowan, "Finite Fourier Transform Theory and Its Application to the Computation of Convolutions, Correlations, and Spectra," Teledyne Industries, Inc., 11 Oct. 1966 [AD 800371].

6. T.G. Stockham, Jr., "High Speed Convolution and Correlation," presented at the Spring Joint Computer Conference of the ACM, Boston, April 1966.

7. General Atronics Corp., "First Quarterly Technical Report on Large Aperture Seismic Arrays," Contract AF19(628)-5981, July 1966, p. 36.

8. M.M. Backus, "Array Research," Texas Instruments, Inc., Contract AF33(657)-12747, 3 June 1965.

9. H.E. Landsberg, J. Van Mieghem (eds.), *Advances in Geophysics*, Adacemic Press, New York, 1962, p. 3.

10. M.I. Skolnik, *Introduction to Radar Systems,* McGraw-Hill Book Co., New York, 1962, pp. 476-477.

11. E.F. Chiburis, "Relative Travel Time Anomalies at LASA and the Location of Epicenters Using 'Shift'," Teledyne Industries, Inc., Contract AF33(657)-15919, 7 June 1966.

DOCUMENT CONTROL DATA · R&D
(Security classification of title, body of abstract and indexing annotation must be entered when the overall report is classified)

1. ORIGINATING ACTIVITY (Corporate author)	2a. REPORT SECURITY CLASSIFICATION
General Atronics Corporation 1200 East Mermaid Lane Philadelphia, Pennsylvania 19118	Unclassified
	2b. GROUP N/A

3. REPORT TITLE

THIRD QUARTERLY TECHNICAL REPORT ON
LARGE APERTURE SEISMIC ARRAYS

4. DESCRIPTIVE NOTES (Type of report and inclusive dates)

None

5. AUTHOR(S) (Last name, first name, initial)

None

6. REPORT DATE	7a. TOTAL NO. OF PAGES	7b. NO. OF REFS
March 1967	60	11

8a. CONTRACT OR GRANT NO. AF 19(628)-5981 b. PROJECT NO. c. d.	9a. ORIGINATOR'S REPORT NUMBER(S) ESD-TR-67-282 9b. OTHER REPORT NO(S) (Any other numbers that may be assigned this report) None

10. AVAILABILITY/LIMITATION NOTICES

11. SUPPLEMENTARY NOTES	12. SPONSORING MILITARY ACTIVITY Directorate of Planning and Technology, Electronic Systems Division, AFSC, USAF, L. G. Hanscom Field, Bedford, Mass. 01730

13. ABSTRACT

A progress report on three topics that were studied during the third quarter of Contract AF19(628)-5981 is presented. Preliminary results on spectral estimates of seismic events are presented and two principal conclusions are suggested: noise prediction is probably not a useful means of reducing the variability of spectral estimates, and, for the one large surface-focus event processed to date, there is a significant amount of signal energy above 4 Hz. The problem of detecting nuclear explosions in the presence of large natural events has also been considered during this period. This problem is discussed here, with the emphasis on the possibility of "steering" nulls at the natural events. Difficulties resulting from the sampled nature of the seismic records and from coda reverberations are also discussed in this context. Finally, the location of epicenters by beam splitting with a LASA is discussed. The technique is described, the sources of error are analyzed, and data from three seismic events are presented.

Security Classification

14. KEY WORDS	LINK A		LINK B		LINK C	
	ROLE	WT	ROLE	WT	ROLE	WT
Signal Processing Seismic LASA Array Theory Spectral Analysis						

INSTRUCTIONS

1. ORIGINATING ACTIVITY: Enter the name and address of the contractor, subcontractor, grantee, Department of Defense activity or other organization (*corporate author*) issuing the report.

2a. REPORT SECURITY CLASSIFICATION: Enter the overall security classification of the report. Indicate whether "Restricted Data" is included. Marking is to be in accordance with appropriate security regulations.

2b. GROUP: Automatic downgrading is specified in DoD Directive 5200.10 and Armed Forces Industrial Manual. Enter the group number. Also, when applicable, show that optional markings have been used for Group 3 and Group 4 as authorized.

3. REPORT TITLE: Enter the complete report title in all capital letters. Titles in all cases should be unclassified. If a meaningful title cannot be selected without classification, show title classification in all capitals in parenthesis immediately following the title.

4. DESCRIPTIVE NOTES: If appropriate, enter the type of report, e.g., interim, progress, summary, annual, or final. Give the inclusive dates when a specific reporting period is covered.

5. AUTHOR(S): Enter the name(s) of author(s) as shown on or in the report. Enter last name, first name, middle initial. If military, show rank and branch of service. The name of the principal author is an absolute minimum requirement.

6. REPORT DATE: Enter the date of the report as day, month, year; or month, year. If more than one date appears on the report, use date of publication.

7a. TOTAL NUMBER OF PAGES: The total page count should follow normal pagination procedures, i.e., enter the number of pages containing information.

7b. NUMBER OF REFERENCES: Enter the total number of references cited in the report.

8a. CONTRACT OR GRANT NUMBER: If appropriate, enter the applicable number of the contract or grant under which the report was written.

8b, 8c, & 8d. PROJECT NUMBER: Enter the appropriate military department identification, such as project number, subproject number, system numbers, task number, etc.

9a. ORIGINATOR'S REPORT NUMBER(S): Enter the official report number by which the document will be identified and controlled by the originating activity. This number must be unique to this report.

9b. OTHER REPORT NUMBER(S): If the report has been assigned any other report numbers (*either by the originator or by the sponsor*), also enter this number(s).

10. AVAILABILITY/LIMITATION NOTICES: Enter any limitations on further dissemination of the report, other than those

imposed by security classification, using standard statements such as:

(1) "Qualified requesters may obtain copies of this report from DDC."

(2) "Foreign announcement and dissemination of this report by DDC is not authorized."

(3) "U. S. Government agencies may obtain copies of this report directly from DDC. Other qualified DDC users shall request through

_____."

(4) "U. S. military agencies may obtain copies of this report directly from DDC. Other qualified users shall request through

_____."

(5) "All distribution of this report is controlled. Qualified DDC users shall request through

_____."

If the report has been furnished to the Office of Technical Services, Department of Commerce, for sale to the public, indicate this fact and enter the price, if known.

11. SUPPLEMENTARY NOTES: Use for additional explanatory notes.

12. SPONSORING MILITARY ACTIVITY: Enter the name of the departmental project office or laboratory sponsoring (*paying for*) the research and development. Include address.

13. ABSTRACT: Enter an abstract giving a brief and factual summary of the document indicative of the report, even though it may also appear elsewhere in the body of the technical report. If additional space is required, a continuation sheet shall be attached.

It is highly desirable that the abstract of classified reports be unclassified. Each paragraph of the abstract shall end with an indication of the military security classification of the information in the paragraph, represented as *(TS)*, *(S)*, *(C)*, or *(U)*.

There is no limitation on the length of the abstract. However, the suggested length is from 150 to 225 words.

14. KEY WORDS: Key words are technically meaningful terms or short phrases that characterize a report and may be used as index entries for cataloging the report. Key words must be selected so that no security classification is required. Identifiers, such as equipment model designation, trade name, military project code name, geographic location, may be used as key words but will be followed by an indication of technical context. The assignment of links, rules, and weights is optional.

Security Classification